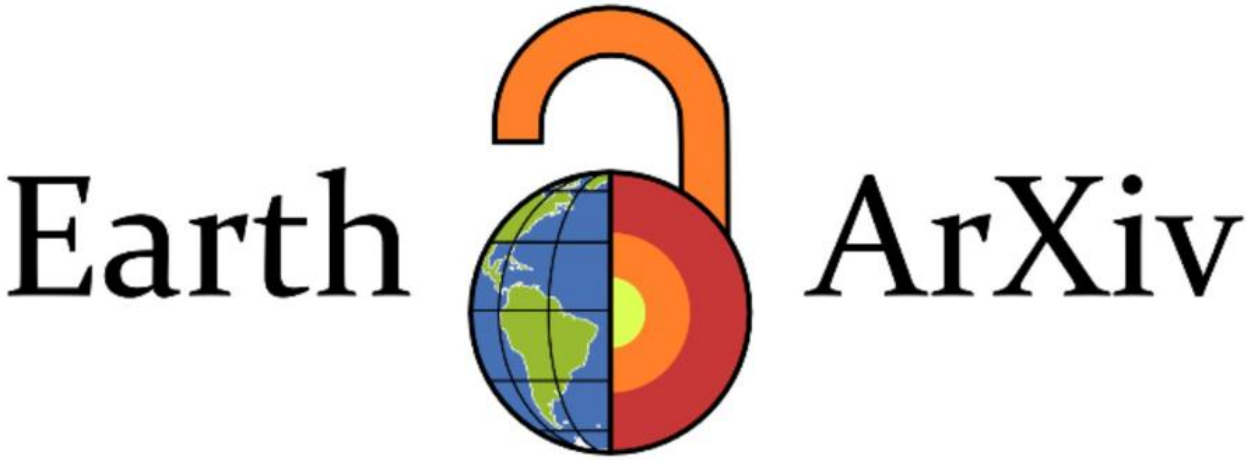

Title Model Construction and Retrospective Validation of Large Earthquake Prediction

Author Zhiyong ZHU

Affiliation Shanghai Institute of Applied Physics, Chinese Academy of Science

E-mail zhuzhiyong@sinap.ac.cn

Peer review status:

This is a non-peer-reviewed preprint submitted to EarthArXiv.

Model Construction and Retrospective Validation of Large Earthquake Prediction

Zhiyong ZHU[1]

Shanghai Institute of Applied Physics, Chinese Academy of Science

Jialuo Rd.2019, 201800, Shanghai, P. R. China

E-mail: zhuzhiyong@sinap.ac.cn

Abstract

Based on the hypothesis that gravity-driven crustal displacement generates earthquakes and facilitates crustal material migration, and following the general law that the velocity of generalized flow in a steady-state system is proportional to the driving force and inversely proportional to the system's internal resistance, a relationship between the frequency of large earthquakes and crustal structure is constructed. And according to Noether's theorems, the connection between large earthquake frequency and crustal energy state is elucidated. The occurrence frequency of large earthquake is therefore proposed to serve as a quantitative measure of the variation of crustal structure and energy state. By analyzing deviations of cumulative number of large earthquake from linearity dependence on time, a method for calculation of occurrence probability for large earthquakes is established, and a "τ" rule method that accounts for both seismic quiescent and active periods for predicting the timing of large earthquakes is also proposed. Retrospective studies show that the time prediction accuracy of both methods is significantly improved compared to predictions based solely on apparent periods. By performing earthquake probability calculations regionally and comprehensively analyzing the results by considering the spatial dependencies between regions, an attempt is made to assess the timing and location of future large earthquakes in certain areas of central mainland China.

Keywords: Earthquake mechanism, Earthquake prediction, Retrospective study, Earthquake frequency, Crustal structure, Crustal energy state

1. Introduction

Earthquakes are one of the most serious natural disasters on Earth [1, 2], causing huge casualties and economic losses almost every year. Countries and regions located near plate boundaries are particularly vulnerable to seismic impacts. The Chinese mainland lies in the southeastern part of the Eurasian Plate; although its inland areas are far from plate boundaries, historical records and seismic archaeology reveal staggering levels of damage caused by earthquakes, In particular, the large

[1] Corresponding author: Zhiyong ZHU (E-mail: zhuzhiyong@sinap.ac.cn)

earthquakes that have occurred since the 20th century (such as the Tangshan earthquake in 1976 and the Wenchuan earthquake in 2008) are still painful memories for countless people. With rapid global economic development, population growth, and ongoing urbanization, the threat of seismic disasters has become severer day by day, and there is a stronger expectation that earthquake prediction will one day become as reliable as weather forecasting.

Modern scientific research on earthquakes by humans can be traced back to the late 19th century, and significant progress has been made over the past century, particularly in earthquake monitoring and theoretical analysis [3–5]. However, these advancements still fall far short of the anticipated goals for earthquake prediction [5, 6], necessitating further in-depth research and continuous summarization of underlying patterns [7–11]. Earthquakes represent a crucial manifestation of structural changes in the crust under stress, indicating that their occurrence patterns are closely linked to crustal structural reconfiguration processes. The present work analyzes the temporal variation trends in accumulation number of large earthquakes (≥7) worldwide and in several seismically active regions since 1980, explores potential mechanisms behind the linear or nonlinear evolution of large earthquake occurrences over time. Based on the linear relationship between large earthquake occurrences and time, a probabilistic prediction method was developed, along with a temporal prediction rule reflecting the temporal characteristics of seismic quiescence and activity periods. These methods were retrospectively validated using historical earthquake data from selected regions of the central mainland China.

2. Observation

The temporal variation patterns of frequency data for large earthquakes (M7 and above) across various regions worldwide were analyzed first. To ensure data completeness and reliability, the study employed data from 00:00 on January 1, 1980, to 24:00 on December 31, 2024, which are reviewed datasets provided by the USGS website [12]. In addition to global data (designated as Zone-1), analyses were conducted for data from several seismically active regions, including most areas of the Chinese mainland and its surrounding regions (designated as Zone-2, longitude: 70.3676 °– 103.322 °, latitude: 25.149 ° – 42.142 °), parts of Northeast Asia (designated as Zone-3, longitude: 130.35 ° – 145.119 °, latitude: 31.7599 ° – 43.752 °), parts of Southeast Asia (designated as Zone-4, longitude: 92.902 ° – 130.791°, latitude: −10.477° – 17.5207 °), Australia and its eastern waters (designated as Zone-5, longitude: 179.791 ° – −179.575°, latitude: −46.676° – −12.41 °), and South America and its surrounding regions (designated as Zone-6, longitude: −119.811° – −23.569°, latitude: −57.5674° – 19.4193 °).

Figure 1 shows the cumulative number of earthquakes of magnitude 7 and above in each region as a function of time. The solid line represents the fitting of the data using equation (1), where N is the cumulative number of M7 and above earthquakes, t is time, and p, q, and t_0 are fitting parameters. When $q = 1$, p is the earthquake frequency. Table 1 presents the value of fitting parameters for each region.

$$N = p \times (t - t_0)^q \qquad (1)$$

As shown in Figure 1 and Table 1, at least based on data from the 45-year period since 1980, the cumulative number of M7 and above earthquakes in the regions studied exhibits an approximately

linear relationship with time. This linear pattern indicates that the annual average occurrence of large earthquakes (earthquake frequency) is a constant across all studied regions. Such a pronounced statistical linearity reflects a certain equilibrium in the internal material structure, state, or acting mechanisms of the Earth's crust, and its underlying mechanism is thought-provoking.

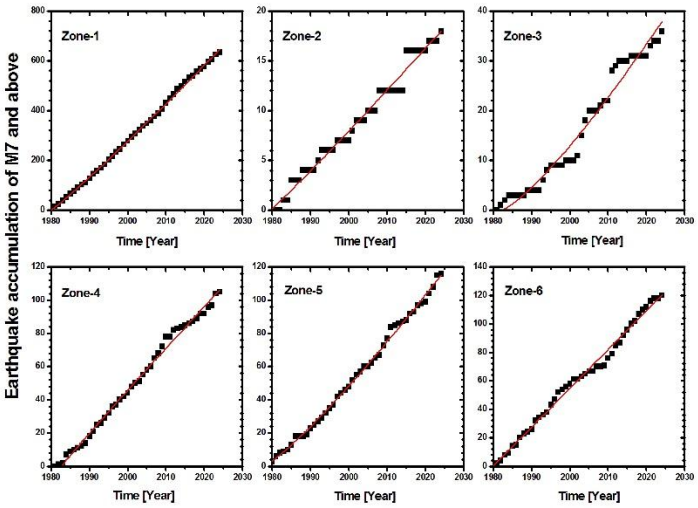

Figure 1. Temporal variation in the cumulative number of M7 and above earthquakes worldwide and in selected regions from 1980 to 2024. The data used are reviewed datasets provided by the U.S. Geological Survey (USGS) website [12].

Table 1. Fitting results of cumulative data of M7 and above earthquakes in the world and selected regions from 1980 to 2024

Zone	p	error	t_0	error	q	error	χ^2	R^2
1	11.14065	0.74034	1980	0.28502	1.07246	0.01646	32.722	0.999
2	0.33092	0.0902	1979.51702	1.17083	1.05225	0.06778	0.515	0.983
3	0.35336	0.20251	1982.35012	2.22469	1.25352	0.14083	4.504	0.968
4	2.9253	0.39698	1982.74204	0.55381	0.96531	0.03502	6.738	0.994
5	1.24217	0.21324	1977.82057	0.751	1.1814	0.04125	4.109	0.997
6	2.70504	0.47077	1979.93464	0.7649	1.00249	0.04349	9.900	0.992

3. Mechanism proposition

Earthquakes are caused by rapid displacement resulting from crustal rupture. Such rupture may result from continuous accumulation of stress and reaching local ultimate strength limits, or from progressive collapse following gradual destruction of the crust's internal structure under repeated low-stress interactions. Considering that the Earth is a near-spherical structure with a solid crust enveloping a fluid mantle, this configuration dictates that the crust is inevitably subjected to the dual effects of inward gravitational force and outward support from mantle material. The Earth's rotation and periodic revolution around the Sun will inevitably subject the crust to long-term periodic impacts from the mantle. These impacts may be directly generated by the mantle or through stress transmission caused by mantle movement. The intensity of such impacts may not be sufficient to

directly cause large-scale fracturing of crustal material, but the repeated long-term effects will cause progressive damage to the crustal structure, thereby creating conditions for large-scale collapse and downward displacement of crustal material under the influence of gravity, leading to large earthquakes.

The structure and composition of each region of the Earth's crust, combined with the external forces acting upon them, determine the maximum amplitude of rupture that can occur in each region during the action period. If the rupture results from a long-term process of periodic external forces, then the upper limit of the maximum possible rupture should also be related to the self-repair capacity of the crustal structure. The existence of a maximum rupture amplitude determines that the maximum earthquake magnitude that can occur in each region of the crust will fluctuate around a most probable value. If the increase in crustal stress causing earthquakes is driven by steady plate movement, or if periodic mantle motion provides the driving force for crustal rupture — in either case — the time required for the maximum structural failure (maximum earthquake) to occur in each region will have an expected value. Provided that the crustal structure does not change significantly with earthquake occurrence, this will render the process of large earthquake occurrence in each region periodic, with the actual period fluctuating around a most probable value due to fluctuations in crustal structure and external forces. This periodic property of large earthquakes determines that the cumulative number of large earthquakes in various regions is linearly related to time.

Due to variations in crustal structure and composition across different locations, as well as potentially different stress magnitudes, the recurrence periods of large earthquakes differ across regions. However, since the cumulative number of large earthquakes in different regions all exhibit linear relationships with time, and the summation of linear relationships remains linear, the pattern of linear increase in cumulative large earthquake counts over time possesses universal applicability. Suppose an analysis region consists of two sub-regions (labeled Region 1 and Region 2), with large earthquake periods of T_{m1} for Region 1 and T_{m2} for Region 2. Then the cumulative number of large earthquakes N_1 in Region 1 over time is $N_1=(t-t_{01})/T_{m1}$, and N_2 in Region 2 is $N_2=(t-t_{02})/T_{m2}$. Hence, the total cumulative number of large earthquakes for the entire region is $N=N_1+N_2=(t-t_0)/T_m$, where $T_m=T_{m1}T_{m2}/(T_{m1}+T_{m2})$, and $t_0=(T_{m2}\times t_{01}+T_{m1}\times t_{02})/(T_{m1}+T_{m2})$. This means that the total cumulative number of large earthquakes in the region will increase linearly with an apparent period of T_m.

If earthquakes are considered to be related to the downward displacement process of crustal material under gravity — that is, during the stress transmission process generated by periodic mantle impacts, the crustal structure is gradually damaged, leading to discontinuous, rapid downward displacement of crustal material and thus producing earthquakes — then according to the general law that the velocity of generalized flow in a steady-state system is proportional to the driving force and inversely proportional to the system's internal resistance, the mass flow intensity I (unit: kg/s) of crustal material downward displacement accompanying earthquakes can be related to the gravitational potential (= g × H, where g is gravitational acceleration in m/s^2, and H is crustal thickness in m) and the resistance to crustal material downward displacement R (i.e., the capacity of the crust to resist earthquake occurrence, abbreviated as seismic resistance, unit: m^2/kg/s) through the following equation:

$$I = m\frac{dN}{dt} = \frac{\mathrm{g}\times\mathrm{H}}{\mathrm{R}} \qquad (2),$$

where m is the downward displacement mass of the crust involved in the earthquake, and dN/dt is the earthquake frequency. Define seismic resistance R = ρ × H/A, where A is the surface area of the landmass involved, and ρ is the seismic resistivity (unit: $m^3/kg/s$), which depends solely on the composition and structure of the crust in that region. Substituting into equation (2) yields:

$$dN/dt = \frac{\mathrm{gA}}{\mathrm{m}\rho} \qquad (3).$$

After integration, we get:

$$N = \frac{\mathrm{gA}}{\mathrm{m}\rho}\times(t - t_0) = (t - t_0)/T_m \qquad (4),$$

$$T_m = \frac{\mathrm{m}\rho}{\mathrm{gA}} \qquad (5)$$

It can thus be seen that for gravity-driven earthquakes, the apparent period T_m (the reciprocal of earthquake frequency) is proportional to the effective mass m of crustal material displaced downward during the earthquake and the seismic resistivity ρ determined by the local crustal structure and composition, while inversely proportional to the gravitational acceleration g and the surface area A of the crustal region involved. For a given region — that is, where surface area and crustal structure and composition are determined (i.e., A and ρ are fixed), and ignoring the minor variations in g within the crustal thickness range — the apparent period T_m is determined solely by the mass m of crustal material displaced downward during the earthquake. The fact that the recurrence period of large earthquakes fluctuates around a most probable value indicates that m should also have a most probable value, in accordance with the most probable magnitude of large earthquakes in the region.

It should be noted that the transport processes of crustal material in different surface regions and at different depths of the crust are not entirely accomplished through brittle fracture (earthquakes). Moreover, crustal displacement caused by earthquakes does not occur solely in the direction perpendicular to the Earth's surface; horizontal displacement also occurs. Therefore, equation (2) expresses only a theoretical relationship for the earthquake-caused material flow process in the direction perpendicular to the Earth's surface. This is based on the hypothesis that earthquakes are produced by periodic mantle impacts damaging the crustal structure and subsequently causing the crust to collapse along the gravitational direction.

For homogeneous crustal blocks with essentially uniform composition and structure, the linear increase of earthquake frequency with area shown in equation (3) is self-evident. For a region with a non-uniform crustal structure, such as a large region consisting of a sub-region with area A_1 and seismic resistance ρ_1 and a sub-region with area A_2 and seismic resistance ρ_2 ($A=A_1+A_2$), with earthquake periods of $T_1 = \frac{m_1\rho_1}{\mathrm{g}A_1}$ and $T_2 = \frac{m_2\rho_2}{\mathrm{g}A_2}$, respectively, one can derive $A/(m\rho) = A_1/(m_1\rho_1) + A_2/(m_2\rho_2)$ with $m\rho$ being the product of the apparent downward displacement mass m and the apparent seismic resistivity ρ of the entire region. In the depth direction, the crustal structure is highly heterogeneous, and due to factors such as temperature variations, large earthquake frequency varies

substantially with depth. In such cases, equation (5) can only describe seismic phenomena within the homogeneous brittle lithosphere, or one may attempt to approximately describe seismic phenomena throughout the entire crustal depth range by using an apparent seismic resistivity, taking it as the thickness-weighted average of the seismic resistivity of various depth zones.

4. Model construction

As shown in equation (5), when the crustal structure and composition of a region are stable (i.e., ρ is a constant), the period of large earthquake in that region is a constant, thus making the cumulative number of large earthquakes linear with time. In this case, we can determine the occurrence probability of future large earthquake based on the deviation of the actual cumulative number of large earthquakes from this linear pattern: if the cumulative number of existing large earthquakes is higher than the theoretical value, it indicates that the local crustal energy is at a low level, and the probability of a large earthquake occurring in the near future is low; whereas if the cumulative number of existing large earthquakes is lower than the theoretical value, it indicates that the crustal energy in that region is at a high level, and the probability of a large earthquake occurring in the near future is high. That is, by statistically analyzing the deviation (residual) data set collected prior to each past large earthquake in a region, a functional relationship between large earthquake occurrence probability and the residual value can be determined. Using this relationship, probabilistic prediction of future large earthquake occurrence can be performed.

To do so, the first thing is to collect the pre-earthquake residual data that is closely related to the occurrence of each historical large earthquake (i.e., the residual data from the year just before each large earthquake occurrence year). Reconfigure the total N_t residual data by subtracting with the minimum residual value and then divide the maximum value (δ_m) of the reconfigured residual into n equal parts starting from 0 to establish n residual levels with the value of $\delta_1=1\times\delta_m/n$, $\delta_2=2\times\delta_m/n$, ……$\delta_n=n\times\delta_m/n=\delta_m$, respectively. Then count the number (N_i) of earthquake events whose reconfigured pre-earthquake residual values are not greater than level δ_i (i=1, 2,……n), forming a data array of (δ_i, N_i). Next, normalize N_i by setting $Y_i=N_i/N_t$, obtaining the normalized data array of (δ_i, Y_i). Since the residual distribution follows normal distribution, the array (δ_i, Y_i) can be approximately fitted by:

$$P = 1 - \frac{1}{1+e^{(x-x_0)/\Delta x}} \qquad (6).$$

This is a special form of the Boltzmann function with a sigmoid curve, capable of reflecting the variation of probability P with variable x. When $x = x_0$, P = 50%; when x is very small, P approaches 0; when x is very large, P approaches 1. Δx reflects the width of the probability distribution. When $x = x_0 - 2.197\Delta x$, the probability is close to 10%; when $x = x_0 + 2.197\Delta x$, the probability is close to 90%. That is to say, if the variable x is the residual value of the number of large earthquakes, then there is an 80% probability that a large earthquake will occur within the range of $x = x_0 \pm 2.197\Delta x$.

Similarly, we can perform statistical analysis on the time interval data collected from previous adjacent large earthquakes in a region to obtain the relationship between the probability of large earthquake and the time interval. The specific approach is to first divide the time intervals into n

levels according to the maximum time interval t_m obtained from previous adjacent large earthquakes, denoted as $t_1=1\times t_m/n$, $t_2=2\times t_m/n$, ……$t_n=n\times t_m/n=t_m$, respectively. Then, counting the number (N_i) of earthquake events that with time interval not greater than level t_i (i=1,2……n), forming a data array of (t_i, N_i). Then normalize N_i by setting $Y_i=N_i/N_m$ (N_m is the total number of time interval data) to obtain the normalized data array of (t_i, Y_i). Usually, the relationship between the probability of large earthquake and the time interval can also be obtained by fitting the data array (t_i, Y_i) with Equation (6). However, if the area under study contains multiple earthquake sequences with far apart mean periods, such as two earthquake sequences with mean periods of x_{01} and x_{02} and distribution width parameters of Δx_1 and Δx_2 respectively, then the data array of (t_i, Y_i) needs to be fitted according to the following formula:

$$P = 1 - \frac{f_1}{1+e^{\frac{x-x_{01}}{\Delta x_1}}} - \frac{f_2}{1+e^{\frac{x-x_{02}}{\Delta x_2}}} \qquad (7).$$

In Equation (7), f_1 and f_2 are the proportions of the number of earthquakes in the two earthquake sequences relative to the total number of earthquakes, i.e., $f_1+ f_2= 1$.

The probability calculated from the time interval between adjacent large earthquakes can reflect the combination of large earthquake series of different periods in the same region, and therefore is expected to provide more information. Because the cumulative number of large earthquakes is related to the energy level of the regional crust, the probability determined by the residual value of the cumulative number of earthquakes is referred to as the energy probability of earthquakes, while the probability determined by the time interval is referred to as the time probability of earthquakes.

5. Applications of the model based on the linearity dependence

China possesses relatively complete historical records of large earthquakes, which can be used to conduct research on large earthquake patterns and retrospective validation of prediction methods. This paper selects large earthquake activity in certain areas of central mainland China as the research subject, with data shown in Table 2. To explore the spatial occurrence patterns of large earthquakes, the whole region is divided from inner to outer into four nested ring-shaped regions according to latitude and longitude (Figure 2), designated respectively as Ring 1, Ring 2, Ring 3, and Ring 4, with area of 250,000 km ², 490,000 km ², 810,000 km ², and 1,210,000 km ², respectively. It is known that 6, 8, 14, and 19 earthquakes of M7 and above occurred in each region respectively between 1879 and 2017 (data from the National Earthquake Data Center NEDC [13]), and all four regions include the M7 earthquake that occurred in Jiuzhaigou, Sichuan in 2017.

Table 2. Large earthquake (M≥7) activity data in selected areas of central mainland China (1879–2017).

time	latitude	longitud	depth	magnitude		location
2017-08-08	33.20	103.82	20	7.0	Ms	Sichuan (Jiuzhaigou)
2013-04-20	30.30	103.00	13	7.0	Ms	Sichuan (Lushan)
2008-05-12	30.95	103.40	19	8.0	Ms	Sichuan (Wenchuan)

1990-04-26	36.04	100.28	8	7.0	Ms	Qinghai
1976-08-23	32.48	104.18	7	7.2	Ms	Sichuan
1976-08-16	32.75	104.10	12	7.2	Ms	Sichuan
1973-02-06	31.36	100.50	7	7.6	Ms	Sichuan
1955-04-14	30.00	101.80	10	7.5	Mw	Sichuan
1954-07-31	38.80	104.20	?	7.0	Ms	Gansu/Inner Mongolia border
1954-02-11	39.00	101.30	35	7.1	Mw	Gansu
1948-05-25	29.50	100.50	?	7.2	Mw	Sichuan
1933-08-25	31.90	103.40	25	7.3	Mw	Sichuan
1927-05-22	37.70	102.20	25	8.0	Ms	Gansu
1923-03-24	31.50	101.00	25	7.2	Mw	Sichuan
1920-12-25	36.60	105.20	?	7.0	Ms	Ningxia
1920-12-16	36.70	104.90	25	8.5	Ms	Ningxia
1904-08-30	31.00	101.10	?	7.0	Ms	Sichuan
1893-08-29	30.60	101.50	?	7.0	Ms	Sichuan
1879-07-01	33.20	104.70	?	8.0	Ms	Gansu

Note: This table presents a subset of recorded large earthquake events. Full data are available from the National Earthquake Data Center (NEDC) [13]. The earthquake record in 1967-08-30 occurred in Sichuan (Luhuo) is confirmed to be with a magnitude of 6.8 and therefore deleted from the list.

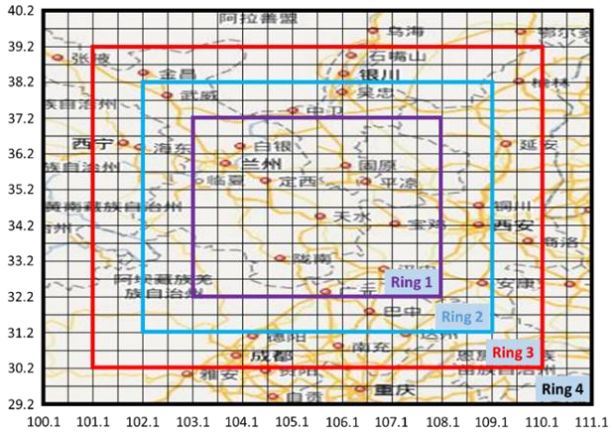

Figure 2. Division of the study area into four nested ring-shaped regions (Ring 1 through Ring 4) in central mainland China. The Chinese characters in the map are the names of provincials and main cities in the area.

According to the linear pattern of cumulative large earthquake counts over time, the cumulative numbers of M7 and above earthquakes that occurred within each ring from 1879 to 2017 were plotted against time, and linear fitting was performed using equation (1) with q = 1 fixed. Based on the deviation of the data from the linear pattern, the relationships between earthquake occurrence probability and residual value for each region were obtained (equation (6)) together with the corresponding parameters (see Table 3). From these relationships and the parameters in Table 3, the

time variation of energy probability of the next M7 and above earthquake occurring after 2017 could be calculated for each region. Meanwhile, based on the time interval data obtained from historical large earthquakes, the relationships between earthquake occurrence probability and time interval for each region were obtained (equation (6) or (7)) together with their parameters (Table 3). From these relationships and parameters, the time probability of the next M7 and above large earthquake occurring in each region in each year after 2017 could be calculated.

Table 3. Fitting parameters for earthquake probability calculations based on actual earthquake occurrence counts for each ring region.

Region in ring#		4	3	2	1	5
Energy Probability	x_0	2.568	2.099	2.208	1.759	2.119
	error	0.024	0.027	0.050	0.032	0.015
	dx	0.459	0.312	0.429	0.154	0.226
	error	0.021	0.024	0.044	0.026	0.013
	χ^2	0.00106	0.002	0.00482	0.00601	0.00165
	R^2	0.994	0.990	0.974	0.975	0.991
Time Probability	f_1	0.63(fixed)	1.0(fixed)	0.57(fixed)	0.4(fixed)	1.0(fixed)
	x_{01}	2.590	9.029	1.927	-3.017	10.232
	error	0.129	0.435	0.310	-	0.230
	dx_1	1.577	6.018	2.978	0.358	4.859
	error	0.115	0.403	0.302	-	0.209
	f_2	0.37(fixed)		0.43(fixed)	0.6(fixed)	-
	x_{02}	14.892		41.784	44.321	-
	error	0.200		0.637	0.957	-
	dx_2	1.308		0.310	5.020	-
	error	0.176		0.907	0.946	-
	χ^2	0.00069	0.00256	0.00069	0.00457	0.00181
	R^2	0.995	0.982	0.994	0.967	0.987

Among the total of 19 large earthquake events involved, two occurred in 1920 with epicenters less than 32 km apart and a time interval of only 9 days, and another two occurred in 1976 with epicenters less than 29 km apart and a time interval of only 7 days. From the perspective of crustal energy, multiple large earthquakes that occur in the same year and at nearby locations should be regarded as a single energy release event. Therefore, when processing the data, large earthquakes less than 32 km apart in the same year may also be treated as a single event. Here, the number of seismic events recorded by energy release is defined as the energy release count of earthquakes, to distinguish it from the actual number of earthquake occurrences. Since the large earthquakes of 1920 and 1976 both occurred within Ring 1, it is necessary to subtract 2 from the actual earthquake counts within each ring to obtain the energy release counts — that is, the energy release counts of large earthquakes occurring within Ring 1, Ring 2, Ring 3, and Ring 4 are considered to be 4, 6, 12, and 17, respectively. Processing data in this way not only yields differences in energy probability calculations, but also in time probability calculations, since the number of zero-time-interval events (i.e., earthquake events

occurring in the same year) differs between the two processing approaches. Table 4 presents the probability parameters for each region obtained by fitting based on energy release counts; notable differences from the data in Table 3 are evident. The impact of the two processing approaches on earthquake prediction will be discussed later.

Table 4. Fitting parameters for earthquake probability calculations based on energy release counts for each ring region.

Region in ring#		4	3	2	1	5
Energy Probability	x_0	2.512	2.011	1.788	1.082	1.590
	error	0.014	0.012	0.018	0.007	0.013
	dx	0.378	0.223	0.295	0.054	0.184
	error	0.012	0.011	0.016	0.007	0.012
	χ^2	0.00041	0.00055	0.00091	0.00159	0.016
	R^2	0.998	0.997	0.995	0.993	0.991
Time Probability	f_1	0.56(fixed)	0.46(fixed)	0.4(fixed)	0.67(fixed)	1.0(fixed)
	x_{01}	3.169	4.890	6.0	41.006	11.231
	error	0.105	0.428	2.0e-6	0.131	0.248
	dx_1	1.188	2.043	0.5(fixed)	0.5(fixed)	4.503
	error	0.092	0.327	-	-	0.223
	f_2	0.44(fixed)	0.54(fixed)	0.6(fixed)	0.33(fixed)	-
	x_{02}	14.677	17.786	41.664	55.012	-
	error	0.147	0.480	0.013	0.266	-
	dx_2	1.443	4.638	0.5(fixed)	0.5(fixed)	-
	error	0.129	0.481	-	-	-
	χ^2	0.00048	0.00098	0.00001	0.00068	0.00226
	R^2	0.997	0.994	1.0	0.997	0.985

Note: dx_1 and dx_2 for time probability in Ring 1 and Ring 2 were artificially fixed at 0.5 due to insufficient data. See text for details.

5.1 Probability analysis

Figures 3–6 compare the linear fitting and probability calculation results obtained from energy release counts and actual earthquake occurrence counts for each region (in the figures, (a) and (b) are obtained from energy release data, while (c) and (d) are calculated from occurrence count data). As can be seen, for the data within Ring 4 and Ring 3, which have relatively larger sample sizes, the two processing approaches yield little difference in results. For the data within Ring 2 and especially Ring 1, which have smaller sample sizes, the processing approach affects both the energy probability and time probability calculations, though it does not affect the overall trend of probability variation. The following discussion will focus primarily on the results obtained from the energy release data processing approach with fitting parameters are shown in Table 4.

Figure 3a shows the linear fit of energy release data from 17 large earthquakes within Ring 4, demonstrating that the data follow a good linear pattern. Figure 3b shows the energy probability and time probability of a large earthquake occurring in this region after 2017. As shown, taking 2017 as

the time of the last M7 and above earthquake in this region, the energy probability of the next large earthquake gradually increases in the coming years, approaching 50% around 2025 and approaching 100% by 2040. The time probability indicates that for a large earthquake that may occur before 2040, there is a 56% chance that it may occur before 2027, and a 44% chance between 2027 and 2039. Figure 4 presents a similar analysis of the 12 magnitude 7 and above events within Ring 3, yielding the energy probability and time probability of the next M7 and above earthquake occurring within Ring 3 (Figure 4b). It can be seen that the energy probability of a large earthquake occurring within Ring 3 before 2025 is very low (below 5%), approaching 50% around 2034 and approaching 100% by 2047. The time probability results for large earthquakes within Ring 3 are similar to those within Ring 4, with nearly a 50% probability of occurring before 2030 and nearly a 50% probability of occurring between 2030 and 2045. As the same with Ring 4, the time probability showing occurrence before and after 2030 do not mean two independent large earthquake events, but rather that a single large earthquake event may occur either before 2030 or after 2030. The energy probability results within Ring 4 show a 50% probability of a large earthquake occurring around 2025, while the energy probability results within Ring 3 show less than a 5% probability before 2025, suggesting that if a large earthquake occurs around 2025, it should occur in the area between Ring 4 and Ring 3.

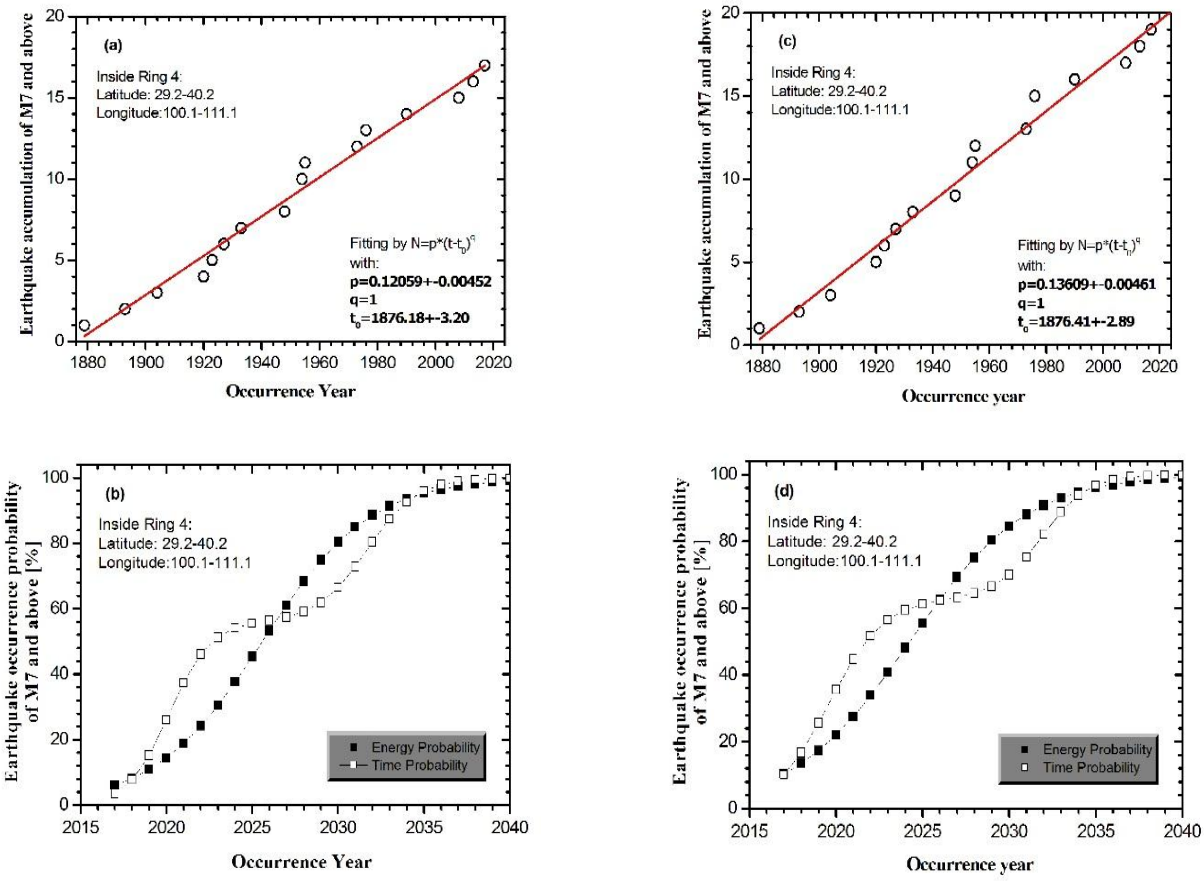

Figure 3. (a) Linear fit of energy release data (17 events) within Ring 4, (b) Energy probability and time probability after 2017 within Ring 4; (c) Linear fit of actual earthquake occurrence data (19 events), (d) Corresponding probability results.

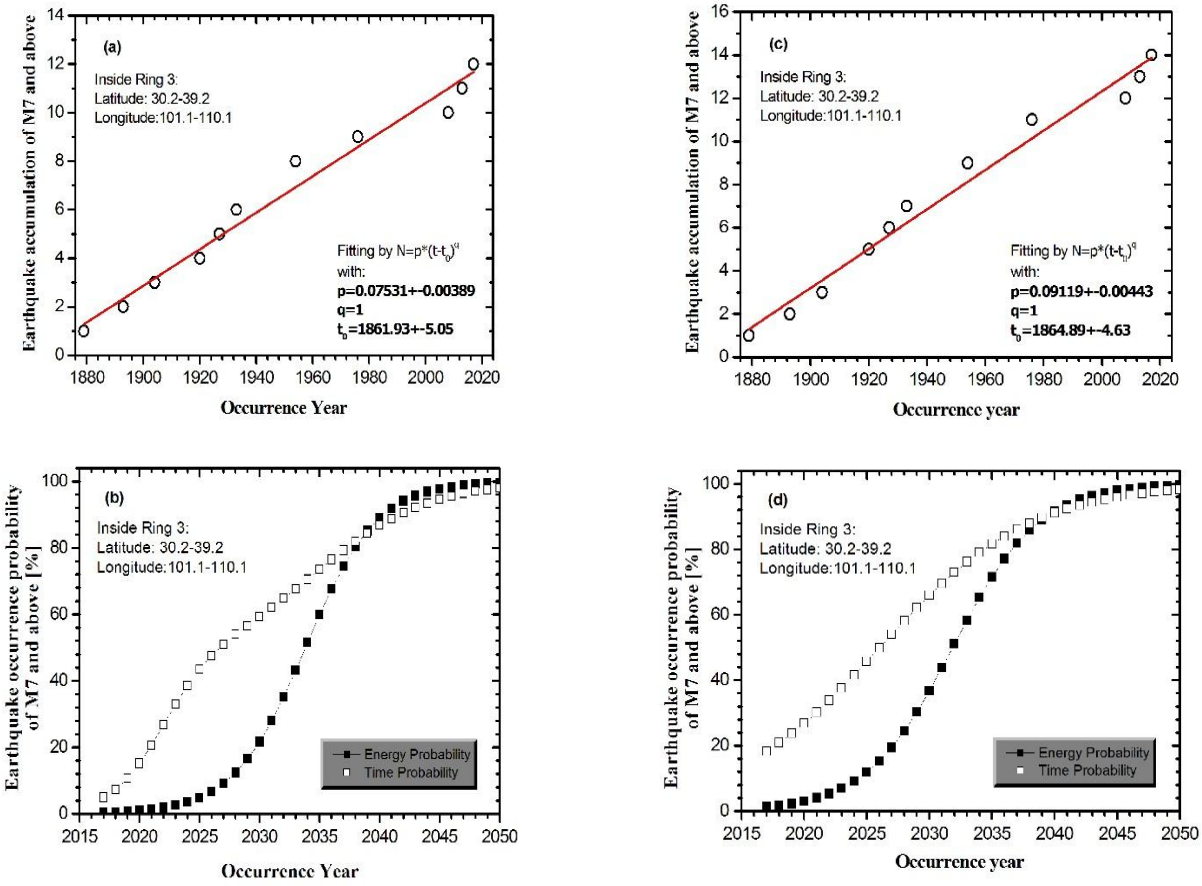

Figure 4. (a) Linear fit of energy release data (12 events) within Ring 3, (b) Energy probability and time probability after 2017 within Ring 3; (c) Linear fit of actual earthquake occurrence data (14 events), (d) Corresponding probability results.

Narrowing the analysis scope to within Ring 2 (490,000 km ²), a linear relationship was fitted to the remaining 6 data points (Figure 5a), from which the energy probability and time probability of the next large earthquake occurring within Ring 2 after 2017 were calculated (Figure 5b, parameters in Table 4). It can be seen that as time increases, the energy probability of a large earthquake occurring in this area will reach 50% by 2034 and approach 100% by 2064. The time probability results show probability jumps in 2025 and 2060. Clearly, these distinct time steps do not indicate more certain earthquake timing, but rather reflect insufficient data such that the expected statistical distribution is absent. The parameters for Ring 1 and Ring 2 listed in Table 4 were obtained by artificially fixing the distribution width parameter at 0.5 in the fitting of time interval data; this does not affect the discussion in this paper.

Continuing the analysis of the Ring 1 area, which covers only 250,000 km ², it was found that the only 4 energy release data points still follow a linear pattern (Figure 6a). The energy probability and time probability of the next M7 and above earthquake occurring in this region after 2017 were thus calculated (Figure 6b). Based on the energy probability and time probability, it is judged that the probability of a M7 and above earthquake occurring within Ring 1 before 2055 is very small,

indicating that M7 and above large earthquakes occurring within Ring 4 before 2055 are likely to occur outside Ring 1. Furthermore, the energy probability results show that the probability of a large earthquake occurring within Ring 1 will reach 50% by 2065 and approach 100% by 2075 (Figure 6b). It is worth noting that the probability results calculated from energy release counts and from actual earthquake occurrence counts differ considerably within Ring 1 (see Figures 6b and 6d). The energy probability distribution calculated from earthquake occurrence counts (Figure 6d) is much broader than that calculated from energy release counts (Figure 6b), because when the successive large earthquakes with close epicenters occurred in 1920 and 1976 are treated as two independent seismic events, the dispersion of the Ring 1 data relative to the linear pattern increases (compare Figure 6c with Figure 6a). From the time probability perspective, counting successive large earthquakes of close location in the same year as independent events greatly increases the proportion of zero-time-interval data in the already small dataset, causing a corresponding increase in probability calculations (see the time probability results in Figures 6d and 6b).

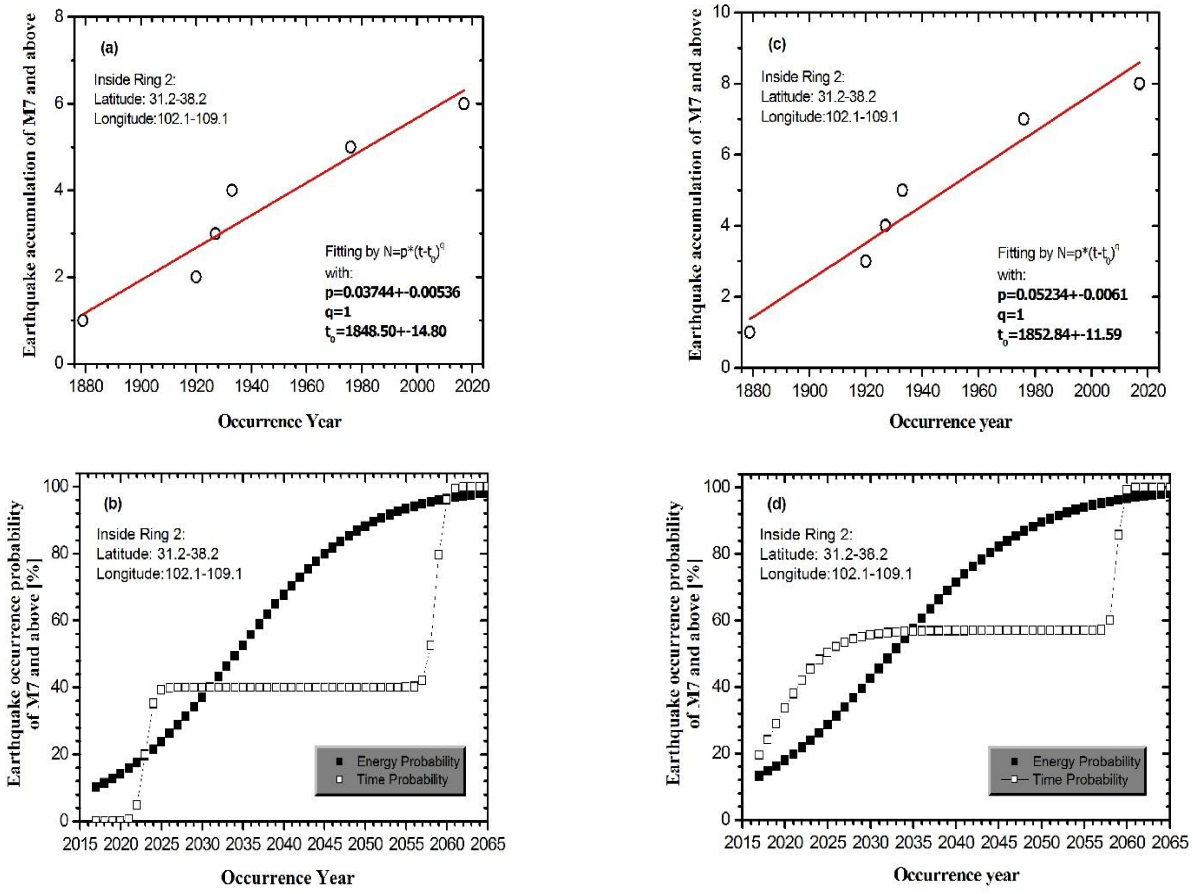

Figure 5. (a) Linear fit of energy release data (6 events) within Ring 2, (b) Energy probability and time probability after 2017 within Ring 2; (c) Linear fit of actual occurrence data (8 events), (d) Corresponding probability results.

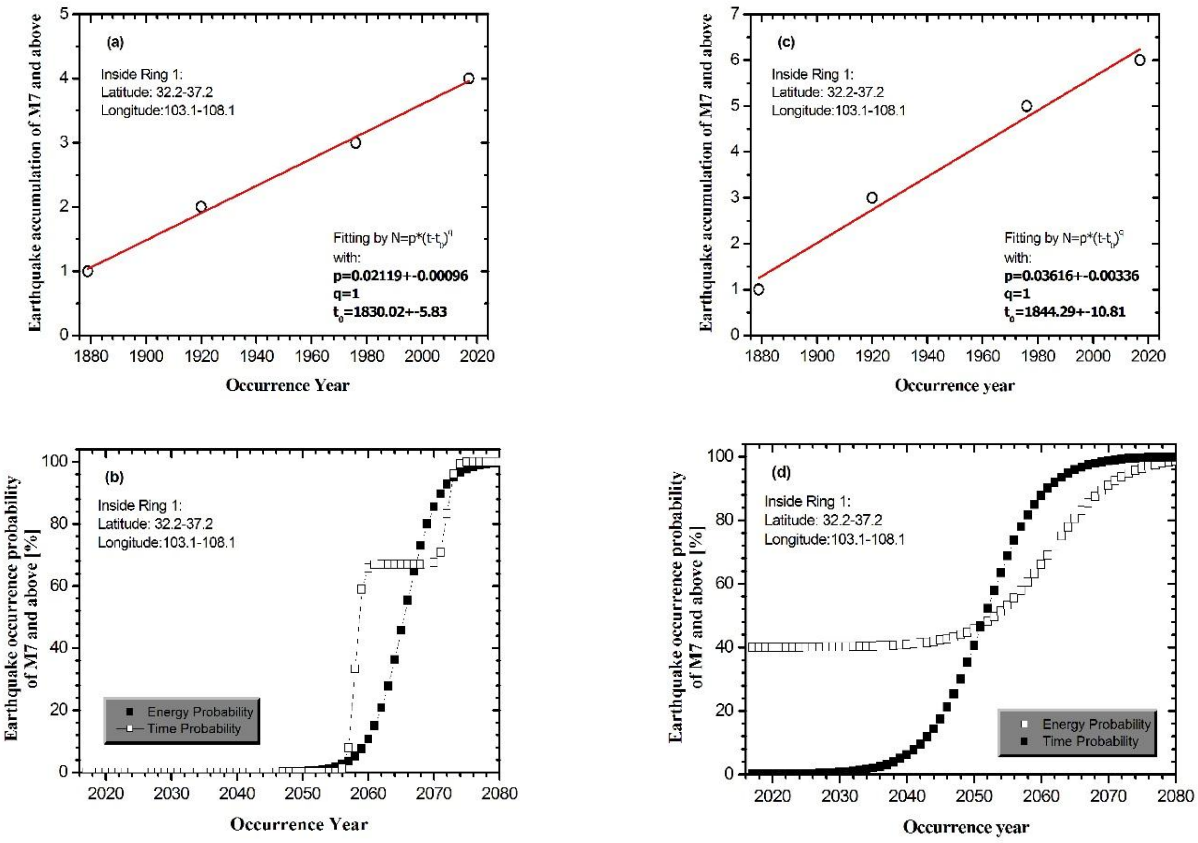

Figure 6. (a) Linear fit of energy release data (4 events) within Ring 1, (b) Energy probability and time probability after 2017 within Ring 1; (c) Linear fit of actual occurrence data (6 events), (d) Corresponding probability results.

The above probability analysis did not consider the spatial distribution of large earthquake events. Figure 7 shows the variation of large earthquake occurrence counts and energy release counts with the surface area of each ring region. As seen, both types of data exhibit approximately linear relationships with area. It looks like that large earthquakes are uniformly distributed in this region. However, if the locations and times of the 19 actually occurring large earthquakes are plotted on the map, as shown in Figure 8, we are surprised to find that the distribution of these large earthquakes is highly uneven and closely related to geographic location. Large earthquake events are very sparse in the Loess Plateau and Inner Mongolia Plateau regions in the north (upper half of the figure), while they are dense in the Qinghai-Tibet Plateau, Sichuan Basin hills, and Yunnan-Guizhou Plateau regions in the south (lower half of the figure). Moreover, 13 of the 19 large earthquakes marked in the figure are concentrated in the southwestern region, meaning that large earthquakes are primarily concentrated in the Qinghai-Tibet Plateau and Sichuan Basin hilly areas. The reason why the number of large earthquakes and the number of earthquake energy releases within each ring show a linear relationship with the surface area of the region (Figure 7) is coincidentally because the regional division here results in a similar area proportion for regions with completely different geological structures in the north and south within each ring (with 34.7 ℃N as the boundary, see Figure 8).

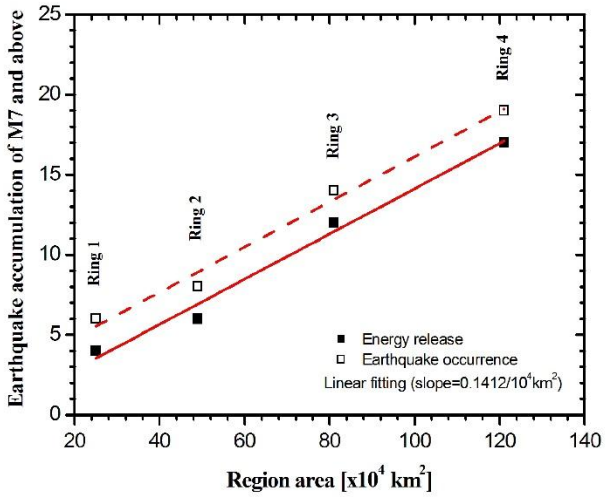

Figure 7. Variation of large earthquake occurrence counts and energy release counts with surface area of each ring region.

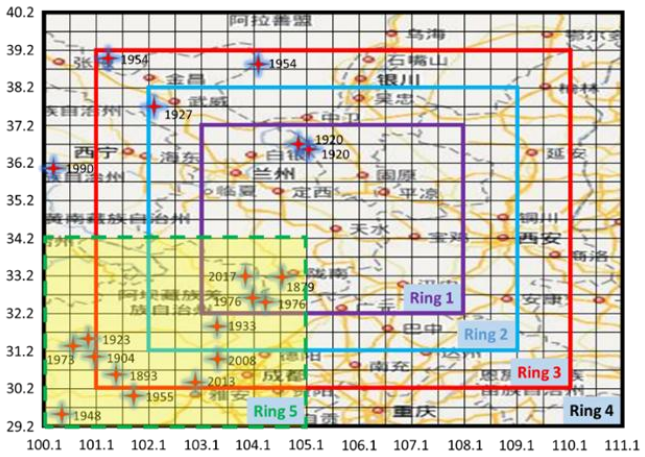

Figure 8. Spatial distribution of the 19 large earthquake events (M≥7, marked with red star) that occurred in the study area between 1879 and 2017. The yellow dashed-line area in the lower-left corner marks Ring 5 (southwestern dense region).

Selecting the 13 large earthquakes (energy release count of 12) from the seismically dense southern region (the 250,000 km ²area in the southwestern part within Ring 4, marked as the dashed-line area in the lower-left corner of Figure 8, designated as Ring 5: longitude 100.1 °–105.1 °, latitude 29.2 °–34.2 °) for data analysis (Figures 9a and 9c), the energy probability and time probability of the next large earthquake occurring in this region after 2017 were obtained, as shown in Figures 9b and 9d (with fitting parameters listed in Tables 3 and 4). The results show that the energy probability of the next M7 and above large earthquake occurring in this region after 2017 will reach 50% in 2036 and approach 100% by 2045 (Figure 9b). Additionally, as seen from Figures 9b and 9d, the time probability results and energy probability results differ notably: the energy probability results indicate a very low probability of a large earthquake occurring in this region before 2030, while the time probability shows a greater than 60% probability of a large earthquake occurring in this region by 2030. Since time probability is calculated solely through statistical analysis of adjacent large

earthquake time intervals without considering the physical correlation between adjacent large earthquakes, whereas energy probability is calculated based on the deviation of earthquake counts from the linear relationship and considers the physical impact of reduced crustal energy after an earthquake on the probability of the next large earthquake, the energy probability data are considered more valuable for reference. That is, the possibility of a M7 and above large earthquake occurring within Ring 5 before 2030 is considered low. In other words, energy probability can further discriminate judgments given by time probability. The same consideration should apply to the situation within Ring 3 before 2025, where time probability is high but energy probability is low (Figures 4b and 4d) — i.e., the possibility of a M7 and above large earthquake occurring within Ring 3 before 2025 is not high.

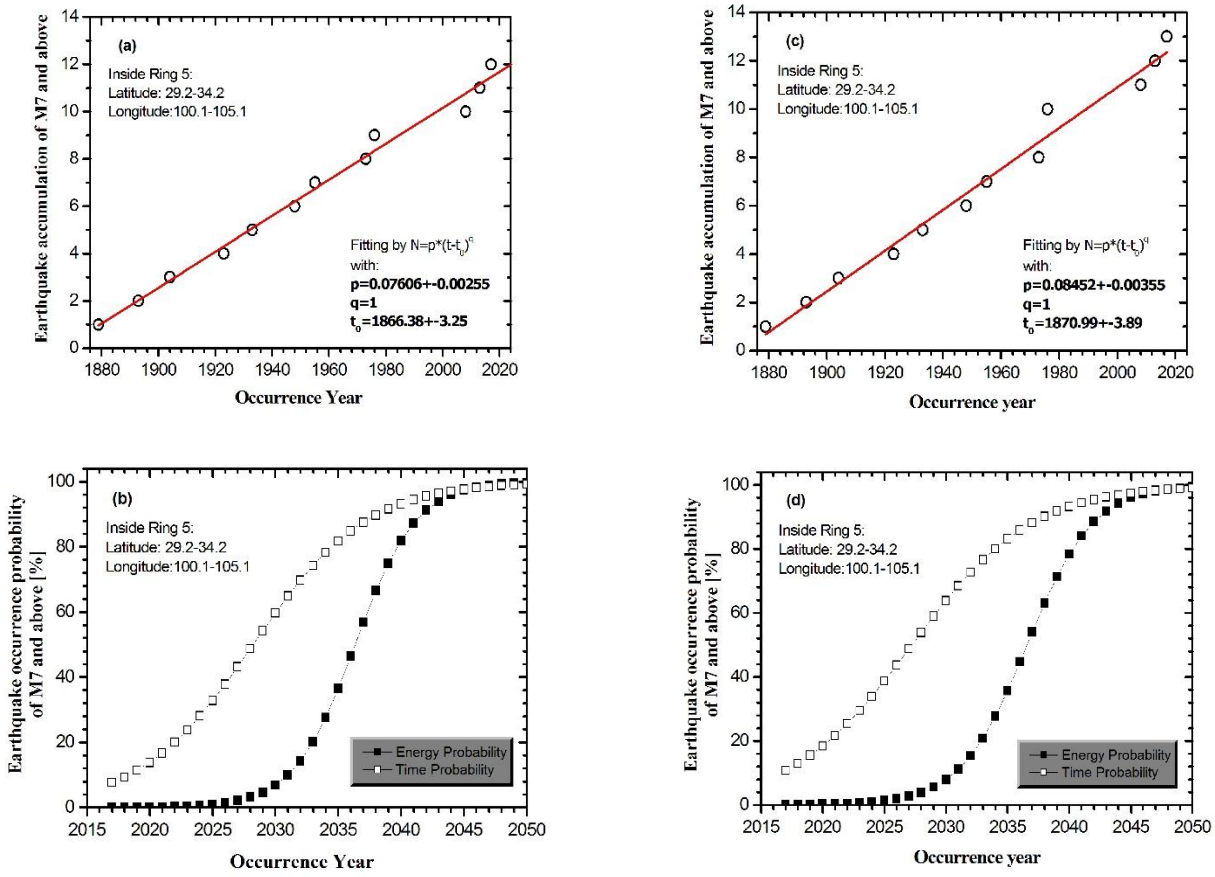

Figure 9. (a) Linear fit of energy release data (12 events) within Ring 5; (b) Energy probability and time probability after 2017 within Ring 5; (c) Linear fit of actual occurrence data (13 events); (d) Corresponding probability results.

5.2 Apparent recurrence time analysis

If the cumulative number of large earthquakes is linearly related to time, then according to equation (4), the apparent period T_m (=1/p) of large earthquakes can be obtained from the large earthquake frequency (i.e., the p value in equation (1) with q=1), which is close to the mean value obtained from statistical analysis of large earthquake time intervals. From this period, the approximate

time of the next large earthquake can be estimated. For example, the apparent period T_m within Ring 4 = 1/0.12059 ≈ 8.3 years (Figure 3a, obtained from energy release counts, same below), within Ring 3 T_m = 1/0.07531 ≈ 13.3 years (Figure 4a), within Ring 2 T_m = 1/0.03744 ≈ 26.7 years (Figure 5a), within Ring 1 T_m = 1/0.02119 ≈ 47.2 years (Figure 6a), and within Ring 5 T_m = 1/0.07606 ≈ 13.1 years (Figure 9a). From these, the approximate times for future large earthquake occurrences in each region after the 2017 earthquake can be estimated, as shown in Table 5. By combining the spatial relationships between regions for comprehensive analysis of earthquake occurrence time data, we can even further infer the approximate locations of these large earthquakes. For instance, in 2025, only in Ring 4 a forthcoming large earthquake is estimated, so the earthquake location can be determined to be between Ring 4 and Ring 3 and outside Ring 5. Similarly, the large earthquake occurring within Ring 4 in 2033, within Ring 3 in 2030, and within Ring 5 in 2030 may belong to the same seismic event, so its location should be between Ring 3 and Ring 2 and within Ring 5 (Table 5), and so on.

Table 5. Approximate times for future large earthquake occurrences in each region after 2017, estimated from apparent periods derived from energy release counts.

Region in ring#			**4**	**3**	**2**	**1**	**5**
Recurrence time (year)			8.3	13.3	26.7	47.2	13.1
Occurrence position expected	4-3	**Occurrence time expected**	2025.3				
	3-2,5		2033.6	2030.3			2030.1
	2-1,5		2041.9	2043.6	2043.7		2043.2
	4-3		2050.2				
	3-2,5		2058.5	2056.9			2056.3
	1, 5		2066.8	2070.2	2070.4	2064.2	2069.4

Notes: Second column note: "4-3" (indicates region between the fourth and third ring), "3-2,5" (indicates region between the third and second ring and within the fifth ring), "2-1,5" (indicates region between the second and first ring and within the fifth ring), "2-1" (indicates region between the second and first ring), "1,5" (indicates region within the first and fifth ring).

As shown in Figure 8, the distribution of large earthquakes within the entire region (Ring 4) is highly uneven. Large earthquakes are sparse in the north (north of 34.7 ℕ) and dense in the south (south of 34.7 ℕ), indicating that the northern and southern regions have different seismic resistivity and large earthquake periods. Given that the large earthquake period of the entire region (Ring 4) is $T_m \approx 8.3$ years, and the large earthquake period of the southern region is $T_{m1} \approx 13.1$ years (equivalent to the large earthquake period within Ring 5, see Figure 8), then from $1/T_m=1/T_{m1}+1/T_{m2}$, the large earthquake period of the northern region $T_{m2} \approx 22.7$ years is obtained. Since the last large earthquake in the northern region occurred in 1990, the next large earthquake in the northern region should have occurred in 2012 (not occurred, failed prediction), and the subsequent one should occur in 2035, and so on.

The above predictions based on apparent periods should not be taken seriously because the apparent period of large earthquakes in a region is merely the statistical average of historical large earthquake time interval data for that region. Considering the wide statistical distribution of time intervals resulting from the alternation of large earthquake active and quiescent periods, it is impossible to give meaningful predictions. Later in the paper it will show that although the prediction

accuracy based on apparent period is low it can be served as a criterion for judging whether other earthquake prediction methods are meaningful.

6. Retrospective validation of the model

6.1 Retrospective study of the probability analysis

To verify the effectiveness of the probability analysis method established in this paper, the historical data listed in Table 2 were used for retrospective validation of prediction accuracy. The approach was to take 1948, 1954, 1955, 1973, 1976, 1990, 2008, and 2013 successively as the time points of the last M7 and above large earthquake in each region, calculate the probability of the next large earthquake occurrence using large earthquake data prior to each of these years, take the year corresponding to a probability value of 50% as the predicted time of the next earthquake, compare it with the actual occurrence time. From the deviation the prediction accuracy was obtained by calculating the ratio of the number of events with time deviations within ±10 years and ±5 years to the total number of events. The way of continuously updating earthquake prediction results with newly occurring earthquake events conforms to the Bayesian principle [14].

Table 6 summarizes the analysis results, including results obtained from earthquake occurrence counts and from energy release counts. Table 6 also presents results obtained from apparent period analysis, and finally provides the probability predictions and apparent period analysis results for future large earthquakes with 2017 as the most recent large earthquake. As shown in the table, the total number of completely independent large earthquake events available for retrospective study is 23, including 6 large earthquake events within Ring 5, 8 within Ring 4, 5 within Ring 3, 2 within Ring 2, and 2 within Ring 1. Data for Ring 1 and Ring 2 are relatively scarce, but considering that the large earthquake frequencies obtained from each retrospective stage in these two regions do not change significantly (see Figure 10), the data from these regions are still considered reliable for evaluation. Figure 10 compares the large earthquake frequencies of different regions at different retrospective stages calculated from actual large earthquake occurrence counts, and also shown are the large earthquake frequencies calculated from all data for each region before 2017. The large earthquake frequency results calculated from energy release counts differ in value from those calculated from earthquake counts (data in Table 6), but the trend of variation is the same.

Table 6. Summary of retrospective analysis results for large earthquake probability predictions and apparent period analysis involving 23 independent large earthquake events across all ring regions.

Data region	Last Earthquake Time in the region	Occurrence frequency (1/year)	Apparent Period (year)	Next Earthquake time expected				proposed	Actually Occurred	
				From apparent period	Deviation Δt (year)	Energy probability 50%	Deviation Δt (year)	position	time	position
Based on the data before 1948										
Ring 5	1948	0.072	13.9	1961	+6	1961	+6	In5	1955	4-3,In5
		0.072	13.9	1961	+6	1961	+6			

Ring 4	1948	0.12684	7.9	1955	+1	1955	+1	In4	1954	3-2,O5
		0.10661	9.4	1957	+3	1957	+3			
Ring 3	1933	0.11175	8.9	1941	-13	1947	-7	In3	1954	3-2,O5
		0.08813	11.3	1944	-10	1947	-7			
Ring 2	1933	0.06723	14.9	1947	-29	1962	-14	In2	1976	In1,In5
		0.04724	21.2	1954	-22	1967	-9			
Ring 1	1920	0.04878	20.5	1940	-36	1953	-23	In1	1976	In1,In5
		0.02439	41.0	1961	-15	1959	-17			
Based on the data before 1954										
Ring 5	1948	s.a.b								
Ring 4	1954	0.13413	7.5	1961	+6	1968	+13	In4	1955	4-3,O5
		0.11668	8.6	1962	+7	1970	+15			
Ring 3	1954	0.11183	8.9	1962	-14	1966	-10	In3	1976	In1,In5
		0.09364	10.7	1964	-12	1969	-7			
Ring 2	1933	s.a.b								
Ring 1	1920	s.a.b								
From the data before 1955										
Ring 5	1955	0.07568	13.2	1968	-5	1971	-2	In5	1973	4-3,In5
		0.07568	13.2	1968	-5	1971	-2			
Ring 4	1955	0.1423	7.0	1962	-11	1972	-1	In4	1973	4-3,In5
		0.12631	7.9	1962	-11	1974	+1			
Ring 3	1954	s.a.b								
Ring 2	1933	s.a.b								
Ring 1	1920	s.a.b								
From the data before 1973										
Ring 5	1973	0.07526	13.2	1986	+10	1985	+9	In5	1976	In1,In5
		0.07526	13.2	1986	+10	1985	+9			
Ring 4	1973	0.13993	7.1	1980	+4	1979	+3	In4	1976	In1,In5
		0.12664	7.9	1980	+4	1982	+6			
Ring 3	1954	s.a.b								
Ring 2	1933	s.a.b								
Ring 1	1920	s.a.b								
From the data before 1976										
Ring 5	1976	0.08331	12	1988	-20	2002	-6	In5	2008	3-2,In5
		0.07868	12.7	1988	-20	1994	-14			
Ring 4	1976	0.14548	6.9	1982	-8	1991	+1	In4	1990	4-3,O5
		0.12947	7.7	1983	-7	1988	-2			
Ring 3	1976	0.10844	9.2	1985	-23	1988	-20	In3	2008	3-2,In5
		0.08778	11.4	1987	-21	1984	-24			
Ring 2	1976	0.06347	15.8	1991	-26	2000	-17	In2	2017	In1,In5
		0.04322	23.1	1999	-18	1997	-20			

Ring 1	1976	0.04091	24.4	2000	-17	2017	0	In1	2017	In1,In5
		0.02046	48.9	2024	+7	2023	+6			
From the data before 1990										
Ring 5	1976	s.a.b								
Ring 4	1990	0.14511	6.9	1996	-12	1998	-10	In4	2008	3-2,In5
		0.12814	7.8	1997	-11	1996	-12			
Ring 3	1976	s.a.b								
Ring 2	1976	s.a.b								
Ring 1	1976	s.a.b								
From the data before 2008										
Ring 5	2008	0.08109	12.3	2020	+7	2017	+4	In5	2013	3-2,In5
		0.07398	13.5	2021	+8	2013	0			
Ring 4	2008	0.13896	7.2	2015	+2	2008	-5	In4	2013	3-2,In5
		0.12248	8.2	2016	+3	2008	-5			
Ring 3	2008	0.0934	10.7	2018	+5	2008	-5	In3	2013	3-2,In5
		0.07554	13.2	2021	+8	2008	-5			
Ring 2	1976	s.a.b								
Ring 1	1976	s.a.b								
From the data before 2013										
Ring 5	2013	0.08216	12.2	2025	+8	2027	+10	In5	2017	In1,In5
		0.07412	13.5	2026	+9	2026	+9			
Ring 4	2013	0.1365	7.3	2020	+3	2017	0	In4	2017	In1,In5
		0.12053	8.3	2021	+4	2017	0			
Ring 3	2013	0.09068	11	2024	+7	2022	+5	In3	2017	In1,In5
		0.07404	13.5	2026	+9	2023	+6			
Ring 2	1976	s.a.b								
Ring 1	1976	s.a.b								
From the data before 2017										
Ring 5	2017	0.08452	11.8	2028		2037		In5	?	?
		0.07606	13.1	2030		2036				
Ring 4	2017	0.13609	7.3	2024		2024		In4	?	?
		0.12059	8.3	2025		2026				
Ring 3	2017	0.09119	11	2028		2032		In3	?	?
		0.07531	13.3	2030		2034				
Ring 2	2017	0.05234	19.1	2036		2033		In2	?	?
		0.03744	26.7	2043		2034				
Ring 1	2017	0.03616	27.7	2044		2052		In1	?	?
		0.02119	47.2	2064		2065				

Note 1: "4-3, O5" (indicates region between the fourth and third ring and outside ring 5), "3-2, In5" (indicates region between the third and second ring and within the fifth ring), "In1" (indicates region within first ring),

"3-2" (indicates region between the third and second ring), "In1, In5" (indicates region within the first and fifth ring), and so on.

Note 2: "s.a.b" (same as before, meaning results are the same as previous calculation in the region).

Note 3: Numbers in red are results from analysis of energy release counts.

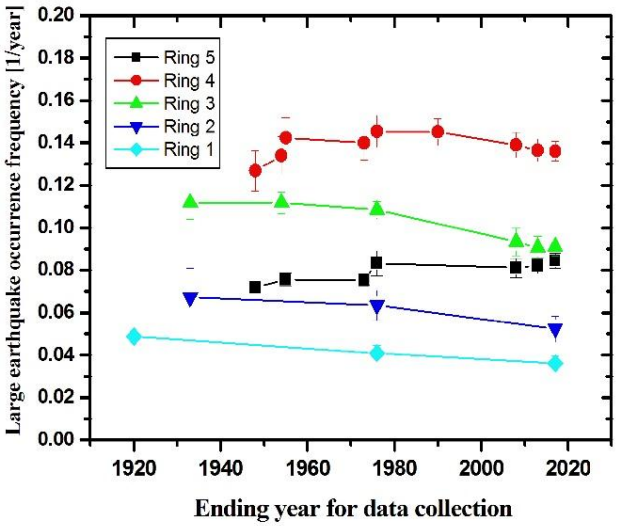

Figure 10. Comparison of large earthquake frequencies of different regions at different retrospective stages, calculated from actual earthquake occurrence counts.

Statistical analysis of the results in Table 6 yields the time prediction accuracy within different allowable deviation ranges. Table 7 compares the accuracy rates from apparent period predictions with those from energy probability predictions (calculated using actual earthquake occurrence counts and energy release counts, respectively), employing two allowable deviation ranges: ±10 years and ±5 years. It is evident that the time prediction accuracy obtained from energy probability is significantly better than that from apparent period predictions. Within a deviation range of ±10 years, the energy probability method yields a time prediction accuracy above 70%, while the apparent period yields a value around 60%. Within a deviation range of ±5 years, the probability prediction yields approximately 40%, while the apparent period prediction yields below 30%.

Table 7. Comparison of time prediction accuracy between apparent period predictions and energy probability predictions.

Way of occurrence time prediction	Accuracy rate (%)			
	From occurrence number analysis		From energy release number analysis	
	Deviation within ±10 year	Deviation within ±5 year	Deviation within ±10 year	Deviation within ±5 year
Based on apparent period	56.5	26.1	65.2	21.7
Value at 50% energy probability	78.3	47.8	73.9	34.7

Figure 11 shows the variation in prediction accuracy when predictions are made using times corresponding to different probability values, with the time prediction accuracy from apparent periods also indicated. The reason why predictions based on the deviation of cumulative earthquake counts from the linear pattern are more accurate than those based on apparent periods may be that the deviation of cumulative earthquake counts from the linear pattern contains information about large earthquake quiescent and active periods. That is, after an earthquake active period, the crustal energy drops to a relatively low level, and the cumulative rate of earthquake counts decreases; when the quiescent period ends, the cumulative rate of earthquake counts increases. These changes are reflected through the deviation of data from the linear pattern, thereby improving the accuracy of earthquake time prediction.

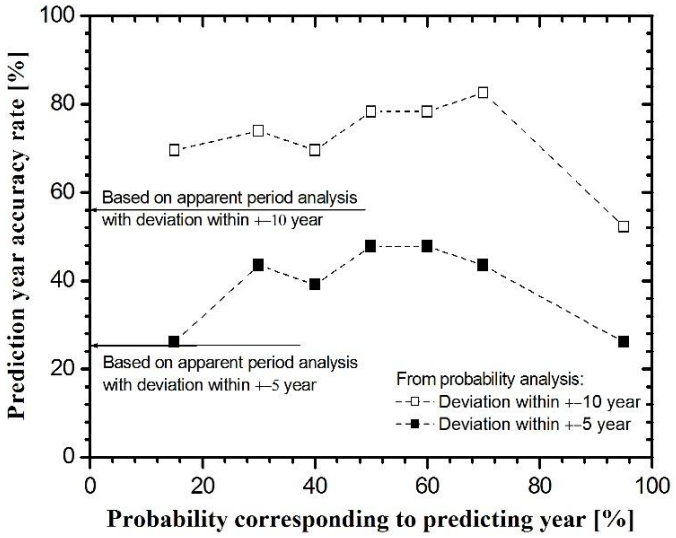

Figure 11. Variation in time prediction accuracy when predictions are made using times corresponding to different probability values. Apparent period accuracy is indicated for comparison.

Subtracting the probability distributions over time of two nested regions of different sizes may yield important information. For example, when the difference between the probability of the larger region and that of the smaller region exhibits a peak, it may indicate that a large earthquake will occur in the area between the larger and smaller regions. When the probability of the larger region is already close to 100%, if the probability of the smaller region begins to increase with time, the difference between the two probabilities will decrease over time, indicating a risk of a large earthquake in the smaller region. If the probability distributions of the two regions are similar, the information provided by the difference is vague; it may indicate that the earthquake event is about to occur in smaller region. Figure 12 shows the results obtained by subtracting the probability distributions over time calculated from data before 1976 within each ring, used to predict the time and location of large earthquakes after 1976. As shown, the probability difference distribution calculated from actual earthquake occurrence counts (blue symbols in Figure 12) differs greatly from that calculated from energy release counts (red symbols), possibly because the overall scarcity of large earthquake data before 1976 caused the different processing approaches for same-year, same-location large earthquakes to have a significant impact on the probability calculation, which is more pronounced within Ring 1 and Ring

2. In the following only the probability results obtained from the energy release approach are discussed.

As shown in Figure 12, the subtraction of probability data obtained from energy release counts between Ring 3 and Ring 2 shows a peak around 1990, and the subtraction between Ring 4 and Ring 5 also shows a peak around 1990, indicating that a large earthquake might occur outside Ring 5 and between Ring 3 and Ring 2. In reality, a large earthquake occurred in 1990 between Ring 4 and Ring 3 and outside Ring 5. When the large earthquake probability in Ring 2 approached 100%, the earthquake probability in Ring 1 began to increase, causing the temporal distribution difference of probabilities between Ring 2 and Ring 1 to decrease after 2014 (Figure 12), indicating that a large earthquake might occur within Ring 1 after 2014. In reality, a large earthquake occurred within Ring 1 in 2017. These facts demonstrate that probability differences can indeed provide information about the timing and location of future large earthquakes. However, the large earthquake that occurred in 2008 between Ring 3 and Ring 2 and within Ring 5 showed no indication in the probability difference distribution obtained from energy release counts. Notably, the subtraction of probability data between Ring 4 and Ring 3 showed a negative peak around 1988, possibly indicating that the probability distribution data of Ring 4 and Ring 3 are very close and cannot provide useful information.

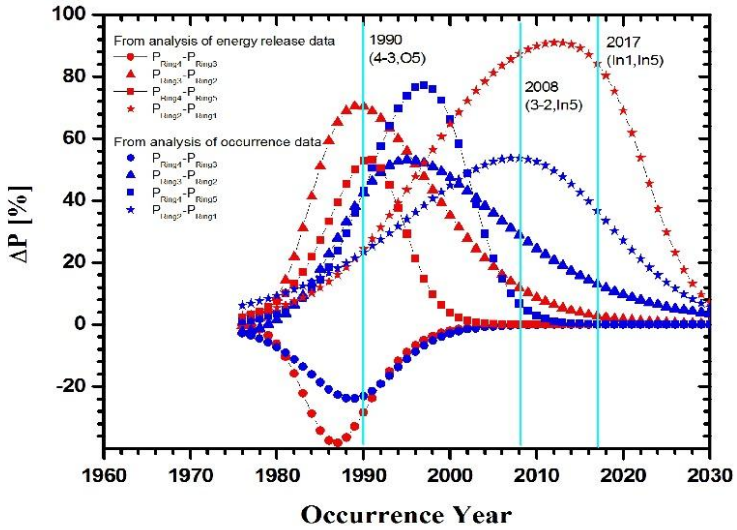

Figure 12. Temporal distribution difference of probabilities between regions calculated from data before 1976, used to predict time and location of large earthquakes after 1976. Blue: from actual occurrence counts; Red: from energy release counts.

Figure 13 shows the results obtained by subtracting the probability distributions over time calculated from data before 2017 within each ring, used to predict the time and location of large earthquakes in this region after 2017. As shown, the temporal distribution difference between Ring 4 and Ring 3 probabilities peaks around 2030, and the temporal distribution difference between Ring 4 and Ring 5 probabilities also peaks around 2030 — does this mean that a M7 and above earthquake will occur around 2030 between Ring 4 and Ring 3 and outside Ring 5? Furthermore, similar to the situation in 1976, due to the wide separation between the probability distributions of Ring 2 and Ring 1 (see Figures 5 and 6), when the large earthquake probability in Ring 2 approaches 100%, the earthquake probability in Ring 1 begins to increase, causing the temporal distribution difference

between Ring 2 and Ring 1 probabilities to decrease after 2056 — does this indicate that a M7 and above earthquake will occur within Ring 1 after 2056? In addition, does the positive peak of the temporal difference between Ring 3 and Ring 2 probabilities in 2040 predict a large earthquake in the area between Ring 3 and Ring 2 around 2040? It is evident that by combining the probability calculation results for each region with the spatial interdependencies between regions, the timing and even location of future large earthquakes can be inferred. Although the earthquake prediction obtained in this manner is still coarse, it has guiding significance for medium- and long-term assessment of future large earthquakes. If combined with local geological structure analysis and small earthquake accumulation process investigation [15], it is expected that the reliability of large earthquake prediction in both time and space can be further improved.

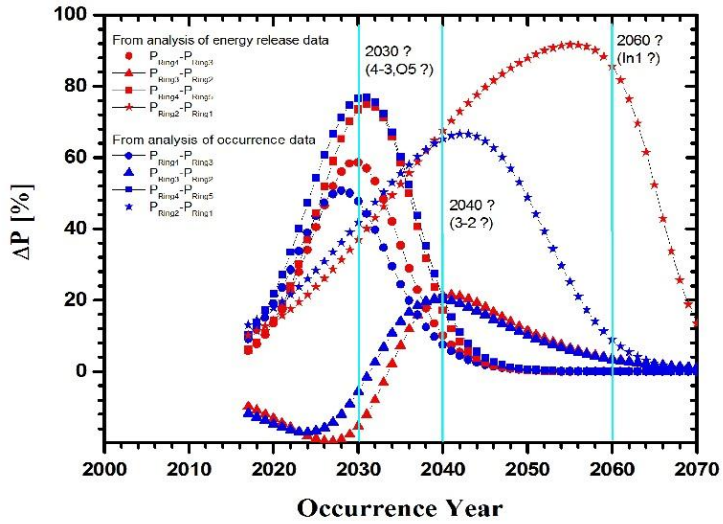

Figure 13. Temporal distribution difference of probabilities between regions calculated from data before 2017, used to predict time and location of large earthquakes after 2017. Blue: from actual occurrence counts; Red: from energy release counts.

6.2 Retrospective study of apparent recurrence time analysis

As mentioned earlier, the prediction accuracy based on apparent periods can be served as a baseline, and any prediction should yield higher accuracy than that from apparent periods to be meaningful. A simple way to improve accuracy is to find a method to distinguish between seismic quiescent and active periods. Here, taking the large earthquake data within Ring 4 from 1879 to 2017 as an example, predictions are first made directly by using the apparent period, and then attempts are made to simulate the quiescent and active period behavior of earthquakes by using combinations of long and short time intervals, with the aim of improving the prediction accuracy of large earthquake time.

Figure 14 shows the prediction of large earthquake occurrence times within Ring 4 based on an apparent period of $T_m \approx 8$ years, where the apparent period value is obtained from energy release counts (see Tables 5 and 6). As shown, the prediction takes 1879 as the starting point, and subsequent predicted times for each large earthquake are obtained by successively adding of 8 years (note: multiple earthquakes in the same year are not taking into account), and the obtained times are

compared with the actual large earthquake occurrence times. Predictions without corresponding actual large earthquakes are classified as false alarms; actual large earthquake events that occurred without prediction are classified as missed alarms; predictions whose time difference from the actual time exceeds the allowable deviation range are classified as error alarms. The total number of events is taken as the sum of the number of predictions and the number of missed alarms, from which the time prediction accuracy rate = number of predictions within the deviation range / total number of events, missed alarm rate = number of missed alarms / total number of events, and false alarm rate = (number of false alarms + number of error alarms) / total number of events. From the statistics in Figure 14, within the ±3-year allowable deviation range, the accuracy rate = 10/20 = 50%, false alarm rate = 8/20 = 40%, and missed alarm rate = 2/20 = 10%; within the ±5-year allowable deviation range, the accuracy rate = 12/20 = 60%, false alarm rate = 6/20 = 30%, and missed alarm rate = 2/20 = 10%.

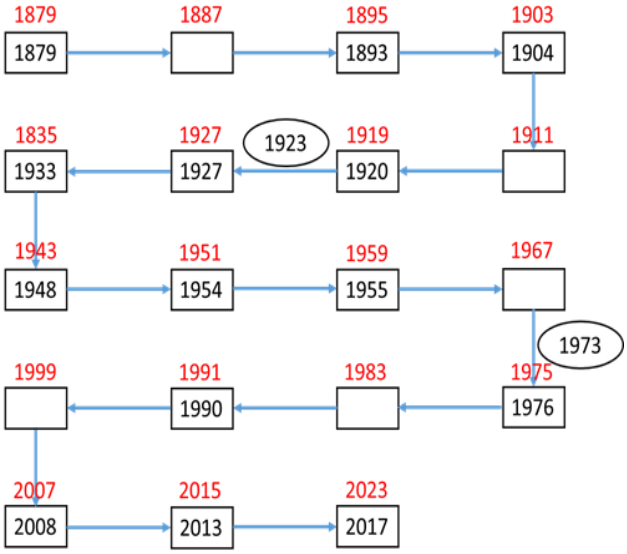

Figure 14. Prediction of large earthquake occurrence times within Ring 4 based on apparent period $T_m \approx 8$ years. Red numbers in square: predicted times; Black numbers in square: actual occurrence times. No number in square: No earthquake occurred, false alarm. The black number in ellipse: actual occurrence time, not predicted earthquake, missed alarm. Multiple earthquakes in the same year are not considered separately.

Compared with the accuracy obtained from apparent periods within the ±5-year allowable deviation range given in Table 7, the accuracy from the method here is much higher. This is because the results in Table 7 were obtained through analysis and synthesis of data from multiple regions (see Table 6), whereas here only the data within Ring 4 are analyzed. Furthermore, the two methods differ in their accuracy assessments. For instance, Table 6 considers that the time determined after 1976 (1976 + 8 = 1984) should be the prediction for the 1990 earthquake, whereas here 1984 is considered an error alarm, and 1984 + 8 = 1992 is considered the prediction for the 1990 earthquake, and so on. Even so, if the data within Ring 4 in Table 6 are statistically analyzed separately, an accuracy of 50% can also be obtained within the ±5-year allowable deviation range (see Table 6, accuracy rate = 4/8 = 50%).

Earthquakes occur in quiescent and active periods. If a time combination can reflect the temporal characteristics of seismic quiescent and active periods, it is expected to substantially improve the

accuracy of earthquake time prediction. Here, a rule is proposed, referred to as the "τ" rule, which contains two provisions: First, it stipulates that the earthquake time interval is a combination of a long time interval τ_l (reflecting the quiescent period) and a short time interval τ_s (reflecting the active period), and the time intervals of large earthquakes repeat in the form $m\tau_l + n\tau_s$, requiring $\frac{m\tau_l+n\tau_s}{m+n} = T_m$ (where n is the total number of time intervals of large earthquakes within a single active period and m is the total number of time intervals within a single quiescent period). Second, the time of the next large earthquake is extended from the time of the last actual large earthquake; if the predicted time of the last large earthquake has no corresponding actual earthquake, the extension is made from the predicted time (note: multiple earthquake occurrences in the same year are not counted separately). Figure 15 shows the predictions made using the "τ" rule for 18 large earthquakes within Ring 4 from 1879 to 2017 (note: there are actually 19 large earthquake events; since 1879 is taken as the prediction starting point, the earthquake of that year is not included in the prediction), where $\tau_l = 2T_m = 2 \times 8 = 16$ years, $\tau_s = T_m/2 = 8/2 = 4$ years, m=1 and n = 2. As shown in Figure 15, total number of events = number of predictions + number of missed alarms = 15 + 4 = 19, number of false alarms = 4 (note that the predictions made in 1927 and 1980 are attributed to false alarms), number of missed alarms = 2, and number of error alarms within the ±3-year allowable deviation range = 0. Therefore, the accuracy of large earthquake time prediction within Ring 4 = 13/19 = 68.4%, false alarm rate = (4 + 0)/19 = 21.1%, and missed alarm rate = 2/19 = 10.5%. Since a large earthquake occurred in 1933 after 1927, according to the second provision of the "τ" rule, subsequent predictions should continue from 1933, yielding a prediction of 1933 + 16 = 1949, therefore the prediction made in the year 1927 is attributed to false alarm. The same is for the prediction made in the year 1980.

It is evident that the accuracy obtained through this method is high, even higher than that obtained from probability calculations. From Table 6, statistical analysis of the data within Ring 4 alone shows that the time prediction accuracy given by probability calculation within the ±3-year allowable deviation range, based on actual earthquake occurrence counts, is only 5/8 = 62.5%. It is unclear whether the high earthquake time accuracy obtained using the "τ" rule is coincidental or has a physical basis. Regardless, using accuracy, false alarm rate, and missed alarm rate as criteria, an optimal time combination (i.e., the optimal τ_l, τ_s, m and n values) can always be found for any region to achieve the best local earthquake time prediction — something easily achievable in today's AI era. Continuing to predict according to this rule, it can be seen that the region should enter a seismic quiescent period after 2017, and the next large earthquake should have a 68.4% probability of occurring within 2017 + 16 = 2033 ± 3 years. This is consistent with the previous probability-based prediction that a large earthquake would occur around 2030 between Ring 4 and Ring 3 and outside Ring 5 (Figure 13).

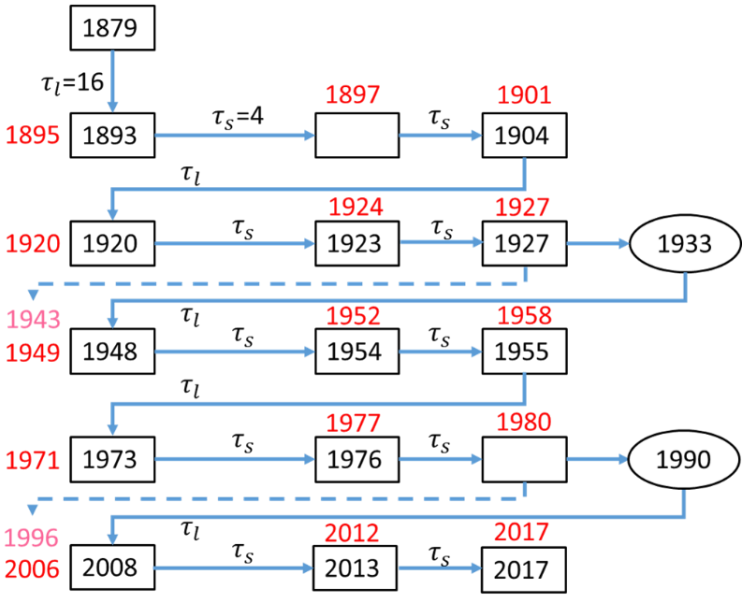

Figure 15. Prediction of large earthquake occurrence times within Ring 4 using the "τ" rule (τ_l = 16 yr, τ_s = 4 yr, m=1, n = 2). Black numbers inside square: actual occurrence times. Red numbers outside square: predicted times. The black number in ellipse: actual occurrence time, not predicted earthquake, missed alarm. Multiple earthquakes in the same year are not considered separately. The 1943 and 1996 earthquake predictions are attributed to false alarms.

7. Discussion

All crustal rupture displacement accompanying large earthquakes contains a horizontal component perpendicular to the direction of gravity and a vertical component parallel to the direction of gravity. Equations (3) and (4) are derived under the assumption that large earthquake occurrence is a downward displacement process of crustal material under the action of gravity with a relationship between crustal material flow and earthquake frequency as described in equation (2). Therefore, they are only applicable to describing the vertical displacement component produced by crustal rupture. The horizontal displacement of crustal rupture is generated by inter-plate interactions and is beyond the scope of this paper. The process of crustal material downward displacement must be accompanied by processes that enable upward displacement of crustal material to maintain the stability of the overall crustal structure and the balance of crustal material, such as volcanic eruptions and lithospheric modification caused by mantle plume activity. These topics are also beyond the scope of this study.

As shown in equation (2), large earthquakes occurring in the crust can be seen as independent quantized events, which flash in different locations in sequence under the action of the gravitational field. The quantum corresponding to a large earthquake can be called a "seismon". Although the occurrence of each large earthquake is mysterious, its frequency is a constant proportional to the gravitational potential. If earthquake events over millions of years are compressed into one year, we should see a continuous flow of crustal material caused by these earthquake events. This is similar to electrons in a conductor. Although the movements of electrons differ from each other under the same

voltage, the current generated by all electron movement exhibits a strong linear relationship with the voltage. That is, with a constant voltage, the average number of electrons passing through the cross-section of the conductor is a constant. While no one knows exactly where each electron will appear on the cross-section, if the observed area is large enough or the observation time is long enough, we will find that the number of electrons passing through that cross-section per unit time is a constant. A similar phenomenon exists with large earthquakes we experience on the Earth's surface. Although the occurrence of a single large earthquake is uncertain in time and space, if we observe a small area for a long time or a large area for a short time, as long as the Earth's crustal structure does not change significantly with the occurrence of earthquakes, we will see a linear relationship between the cumulative number of large earthquakes and time.

Under the premise that the stress state of the crust does not undergo major changes, whether the linear relationship between cumulative large earthquake counts and time shown in equation (4) can be maintained over the long term depends on whether the crustal structure and composition remain stable — that is, whether the seismic resistivity ρ can remain unchanged. If the crustal structure and composition do not change significantly over a period of seismic activity, we can analyze the trend of future large earthquakes based on the linear relationship. However, changes in crustal structure are an inevitable consequence of earthquakes. As the number of earthquakes increases, the crustal structure and even its composition will inevitably undergo significant changes, at which point the seismic resistivity will change with time, and correspondingly the large earthquake frequency will also change with time. When the large earthquake frequency decreases year by year, it indicates a continuous increase in seismic resistivity ρ, suggesting that the crustal strength in the region may be enhanced by the earthquake induced structural changes — somewhat analogous to the work-hardening process in materials. When the large earthquake frequency increases year by year, it indicates that the seismic resistivity is decreased, implying that the crustal structure may undergo accelerated destruction. As can be seen, the relationship between earthquake frequency and seismic resistivity enables us to monitor the changes in the crustal structure of a region from the observation of local large earthquake occurrence.

Furthermore, changes in the frequency of large earthquakes are also related to changes in the energy state of a regional crust. When earthquakes occur periodically, this indicates that seismic events possess translational symmetry in time. According to Noether's theorem [16], temporal translational symmetry corresponds to energy conservation. That is to say, periodic earthquakes imply that the crust is in an energy-stable state, meaning that the energy entering and leaving the crust is balanced. Another implication of this statement is that if the periodicity of earthquakes changes—that is, if the frequency of earthquakes changes—then the energy entering and leaving the crust is no longer in balance, and the energy state of the crust will change. Based on the first law of thermodynamics [17], the annual change in the internal energy of the crust, $\frac{d\Delta U}{dt}$, equals the difference between the annual energy entering the crust, $\frac{dE_i}{dt}$, and the annual energy released through the crust, $\frac{dE_o}{dt}$, i.e.,

$$\frac{d\Delta U}{dt} = \frac{dE_i}{dt} - \frac{dE_o}{dt} \qquad (8).$$

The annual energy entering the crust is approximately constant, determined by celestial motions and crustal material properties, while the release of crustal energy should primarily occur through earthquakes.

As previously discussed, the maximum possible earthquake magnitude in a region has a most probable value. Based on the exponential relationship between the number and energy of small and large earthquakes [18], it can be derived that the total energy released by all earthquakes in gestation of a largest earthquake in a region through seismic waves is given by $E_t \approx \frac{E_m}{1-10^{-(1.5-b)}}$, where 1.5-b>0, E_m is the most probable value of the maximum earthquake energy in the region, corresponding to the most probable magnitude, and *b* is the b-value in the Gutenberg–Richter relation [18]. It can be seen that the total energy released by the crust through seismic waves is a multiple of the most probable value of the maximum earthquake energy in the region. Moreover, since the total energy released by a single earthquake is proportional to the energy released by its seismic waves [19], the total annual energy released through earthquakes is then given by $\frac{dE_o}{dt} = \beta E_m \frac{dN}{dt} = \beta E_m p$, where β is a coefficient, *N* is the number of large earthquakes, and $p = dN/dt$ is the frequency of large earthquakes. Thus, $\frac{d\Delta U}{dt} = \frac{dE_i}{dt} - \beta E_m p$. Assuming that when $p = p_0$, the net energy flow into and out of the crust is zero, i.e., $\frac{d\Delta U}{dt} = 0$, then $\frac{dE_i}{dt} = \beta E_m p_0$, and therefore:

$$\frac{d\Delta U}{dt} = \beta E_m (p_0 - p) \qquad (9),$$

and

$$\Delta U = \int \beta E_m (p_0 - p) dt = \beta E_m \sum_{i=1}^{n} (p_0 - p_i) \Delta t_i \qquad (10).$$

Similar relation can be derived directly from the first law of thermodynamics [17] by taking the volume change ΔV of crust being proportional to the change in earthquake numbers.

It can be seen that when $p > p_0$, ΔU is negative, and the crust releases energy. When $p < p_0$, ΔU is positive, and the crust absorbs energy. The energy absorption or release associated with changes in the crustal energy state is achieved through the reconfiguration of the crustal structure. When earthquake frequency increases, the crustal structure undergoes accelerated destruction to lower the crustal energy state; when earthquake frequency decreases, the crustal structure gradually raises the crustal energy state through slow repair. It can thus be seen that by monitoring the frequency of large earthquakes, one can simultaneously determine changes in both crustal structure and energy state.

The relationship between large earthquake frequency and seismic resistivity established in this paper is based on the hypothesis that gravity generates large earthquakes. However, for structurally stable spherical crust, gravity alone can hardly produce crustal rupture. This necessitates reiterating a previously proposed viewpoint [15]: the periodic motion state of the Earth's rotation and revolution around the Sun will inevitably subject the interior of the crust to long-term, direct or indirect periodic stress caused by mantle fluidity. Even if the intensity of such stress is not high, the repeated long-

term action will cause damage to the crustal structure, thereby creating conditions for the downward displacement of crustal material under the action of the gravitational field. That is, periodic stress induced by mantle activity leads to the destruction of crustal structure; the destruction of crustal structure causes the crust to undergo rupture displacement under the action of the gravitational field; the rapid relative movement between ruptured crustal blocks produces earthquakes. All of this is analogous to a tall building that undergoes overall collapse after its bottom structure is gradually destroyed, causing vibration while simultaneously achieving the migration of material from high gravitational potential regions to low gravitational potential regions. The destruction of crustal microstructure by mantle activity makes it possible for gravity to generate large earthquakes, while the modification of regional macro-structure by large earthquake occurrence determines a region's capacity to resist large earthquakes. The magnitude of seismic resistivity and its variation over time determine the frequency of large earthquakes in that region and its relationship with time.

Compared with the Earth's lifespan of billions of years, the earthquake data obtained by humanity over the past 100-plus years is far from sufficient to reveal the mechanisms of earthquakes. All speculations about earthquake mechanisms, no matter how reasonable, carry the suspicion of being like the blind men touching an elephant. For people today, the most important thing is to master an effective method for earthquake prediction — even without understanding the underlying mechanism — as long as it meets the needs of earthquake prevention and disaster reduction. One of the most direct ways to improve earthquake prediction accuracy is to fully utilize the temporal patterns of seismic quiescent and active periods (if such patterns exist). The reason why the probabilistic prediction method established in this paper, which uses the deviation of cumulative large earthquake counts from the linear pattern, has higher accuracy than predictions based on apparent periods is that the deviation data of cumulative earthquake counts from the linear pattern implicitly contain information about seismic quiescent and active periods. The "τ" rule prediction of earthquakes is the most direct simulation of the temporal characteristics of seismic quiescence and active periods. During quiescent periods, earthquake frequency decreases and the crust absorbs energy; during active periods, earthquake frequency increases and the crust releases energy. Assuming that after experiencing a complete quiescence period and active period, the total energy change of the crust is zero—that is, as shown in equation (10), $\Delta U = \beta E_m \sum_{i=1}^{n}(p_0 - p_i)\Delta t_i = 0$, then within such a time interval:

$$\sum_{j=1}^{m}(p_0 - p_j)\tau_l + \sum_{i=1}^{n}(p_0 - p_i)\tau_s = 0 \qquad (11).$$

Here p_0 is the baseline frequency of large earthquake in the region, in relation to apparent period T_m; p_j is the earthquake frequency in the quiescent period with the time interval of τ_l; and p_i is the earthquake frequency in the active period with the time interval of τ_s, i.e., $p_0 = 1/T_m$, $p_j = 1/\tau_l$, and p_i=1/τ_s. Then we have:

$$m \times \left(\frac{1}{T_m} - \frac{1}{\tau_l}\right) \times \tau_l + n \times \left(\frac{1}{T_m} - \frac{1}{\tau_s}\right) \times \tau_s = 0 \qquad (12),$$

from which it is derived that:

$$T_m = \frac{m\tau_l + n\tau_s}{m+n} \qquad (13),$$

where *m* is the number of time intervals in the seismically quiescent period, and *n* is the number of time intervals in the seismically active period. As can be seen, equation (13) is precisely an important constraint condition of the "τ" rule. It should be noted that, although large earthquake frequency in a single quiescent and active period varies around the baseline frequency and it brings almost no change to the crustal energy state, it is foreseeable that after sufficient long time earthquake interactions the crustal structure will change and the large earthquake frequency will deviate permanently from the original baseline frequency. Let's rewritten Eq.(1) as follows:

$$N = p \times (t - t_0)^q = p \times (t - t_0)^{q-1} \times (t - t_0) = p^* \times (t - t_0) \qquad (14)$$

where $p^* = p \times (t - t_0)^{q-1}$ (for $t - t_0 \geq 1$) being the apparent occurrence frequency of large earthquake of the region. Taking $p^* = p = p_0$ at $t - t_0 = 1$, i.e., taking the occurrence frequency of the first year as the baseline frequency of large earthquake, we have:

$$p^* = p_0 \times (t - t_0)^{q-1} \qquad (15)$$

and then

$$\frac{p_0 - p^*}{p_0} = 1 - (t - t_0)^{q-1} \qquad (16)$$

From the parameters listed in Table 1, we can calculate the occurrence frequency variation in the past 45 years since 1980 by using eq.(16). It is found that for zone 1 to zone 6 the frequency variations are -31.8%, -22.0%, -162.5%, +12.4%, -99.5% and -0.95%, respectively. Negative value means that the crustal in the region releases energy whereas positive value means that the crustal absorbs energy. The occurrence frequency of large earthquake in zone 3 and zone 5 show much larger relative deviations from the baseline value compared to other zones implying that the crustal structures of Northeast Asia as well as Australia and its eastern waters have suffered greater changes compared to other areas during the past 45 years since 1980.

That retrospective predictions using the "τ" rule for large earthquake data improve accuracy is within expectations, but it is somewhat surprising that a simple time combination of "$m\tau_l + n\tau_s$" can yield a time prediction accuracy approaching 70% (±3-year allowable deviation range). If such high-accuracy time combinations are widespread, does this imply that the Earth's crust possesses a structural characteristic of "short-range order and long-range disorder"? Just like macromolecules, where complex macromolecular aggregates are constructed through infinite repetition of monomer molecules? Perhaps single large earthquake merely reflects the local crustal structure, whereas large number of large earthquakes can reflect the form of combination of crustal structures in the region. The method of performing probability calculations regionally and combining them with inter-regional spatial dependencies for comprehensive analysis of the time and location of future large earthquakes has significant application value. It is anticipated that artificial intelligence technology will play an important role in searching for optimal time combinations for regional large earthquakes and in the spatiotemporal coupling prediction of regional large earthquakes.

8. Summary

The rupture and displacement of the crust can be divided into horizontal and vertical components. The horizontal component is determined by the interaction between plates, while the vertical

component is determined by the gravity of the plates themselves. The present work relates the process of crustal rupture and earthquake generation under the action of gravity to the migration of crustal materials. Based on the universal law that the velocity of generalized flow in a steady-state system is proportional to the driving force and inversely proportional to the internal resistance of the system, a relationship between earthquake frequency and seismic resistivity (determined by the structure and composition of the crust) is established. Furthermore, the relation between earthquake frequency and crustal energy state is elucidated according to Noether's theorem. When the crustal structure is relatively stable, the frequency of large earthquakes does not change over time. At this time, the possibility of future large earthquakes can be predicted based on the linear law of the cumulative number of large earthquakes over time. When the frequency of large earthquakes increases over time, it indicates that the local crustal structure is undergoing significant damage, and the crustal energy state is decreasing; conversely, when the frequency of large earthquakes gradually decreases over time, it indicates that the local crustal structure is gradually strengthening, and the crustal energy state is gradually increasing. This close interrelationship lays the physical foundation for the frequency of large earthquakes as a quantitative measure of crustal structure and energy state.

Using the linear pattern of cumulative large earthquake counts over time, historical large earthquake data from certain areas of central mainland China were analyzed. An energy probability calculation method for earthquakes was established based on the deviation of cumulative large earthquake counts from the linear pattern. Through regional probability calculations combined with comprehensive analysis of inter-regional spatial dependencies, an exploratory assessment of the time and location of future large earthquakes in each region was conducted. Meanwhile, a "τ" rule simulating the temporal characteristics of seismic quiescent and active periods was proposed to improve the accuracy of large earthquake time prediction.

The study concludes that the accuracy obtained from apparent period predictions can serve as a criterion for judging the effectiveness of other earthquake prediction methods. The alternation of seismic quiescent and active periods is a concrete manifestation of changes in earthquake frequency, and thus a concrete manifestation of changes in regional crustal energy state. The study finds that simulating the temporal characteristics of seismic quiescent and active periods can effectively improve earthquake prediction accuracy. The deviation data of cumulative large earthquake counts from the linear pattern implicitly contain the temporal characteristics of large earthquake quiescent and active periods; therefore, the probability calculation method established through deviation analysis can significantly improve the prediction accuracy. Retrospective studies using the "τ" rule on large earthquake data in the central region of mainland China (within Ring 4) show that simple time combinations can even increase large earthquake time prediction accuracy rate to approximately 70%. The method of performing probability calculations regionally and combining them with inter-regional spatial dependencies for comprehensive analysis of the time and location of future large earthquakes is operationally feasible. It is believed that artificial intelligence technology will play an important role in searching for optimal time combinations for regional large earthquakes and in the spatiotemporal coupling prediction of regional large earthquakes.

References

[1] Utsu T., A list of deadly earthquakes in the world: 1500-2000., In: International handbook of earthquake and engineering seismology, Part A, San Diego: Academic Press, 2002,691-717

[2] Engdahl E.R., Villasenor A., Global seismicity: 1900-1999, In: International handbook of earthquake and engineering seismology, Part A, San Diego: Academic Press, 2002,665-690

[3] Keilis-Borok V. I., Soloviev A.A. (Eds.), Nonlinear dynamics of the lithosphere and earthquake prediction, Springer-Verlag Berlin Heidelberg 2003, ISSN 0172-7389, ISBN 978-3-642-07806-4

[4] Jordan T. H., Operational earthquake forecasting---State of knowledge and guidelines for utilization, **Annals of Geophysics**, 54(4)(2011)316-384 and references therein

[5] Ullah Sh., Bindi D., Pilz M., Danciu L., Weatherill G., Zuccolo E., Ischuk A., Mikhailova N. N., Abdrakhmatov K., Parolai S., Probabilistic seismic hazard assessment for central Asia, **Annals of Geophysics**, 58(1)(2015)S0103; doi: 10.4401/ag-6687

[6] Main I., Statistical Physics, Seismogensis, and Seismic Hazard, **Reviews of Geophysics**, 34(4)(1996)433-462 and references therein.

[7] Geller R.J., Jackson D.D., Kagan Y.Y., Mulargia F., Earthquakes cannot be predicted, **Science**, 275(14)(1997)1616-1617 and references therein

[8] Wyss M., Cannot earthquakes be predicted? **Science**, 278(17)(1997)487 and references therein

[9] Aceves R. L., Park S. K., **Science** 278(17)(1997)488 and references therein

[10] Geller R.J., Jackson D.D., Kagan Y.Y., Mulargia F., **Science**, 278(17)(1997)488-489 and references therein

[11] Kangan Y.Y., Are earthquakes predictable? **Geophys. J. Int.**, 131(1997)505-525 and references therein

[12] https://www.usgs.gov/programs/earthquake-hazards

[13] https://data.earthquake.cn/datashare/report.shtml?PAGEID=earthquake_lsdz

[14] Bayes T., An essay towards solving a problem in the doctrine of changes. **Philosophical Transactions of the Royal Society of London**, 53(1763)370-418

[15] Zhu Z.Y., Large earthquakes: a way of formation and prediction, https://chinaxiv.org/abs/202511.00162 and https://doi.org/10.31223/X5WT95

[16] Noether E., Invariant Variational Problems, In: The Noether Theorems. Sources and Studies in the History of Mathematics and Physical Sciences, Springer, New York, NY, 2011, https://doi.org/10.1007/978-0-387-87868-3_1

[17] Fermi E., Thermodynamics, New York: Dover Publications, Inc., 1956, ISBN: 978-0486603612 / 048660361X

[18] Gutenberg, Richter, Magnitude and energy of earthquake, **Ann Geofis**, 1956, 9:1-15. Republished in: **Annals of Geophysics**, 53(1)(2010)7-12, doi:10.4401/ag-4588

[19] Encyclopedia of solid earth geophysics, Eds. Harsh.K.Gupta, 2019, Springer Cham, Series ISSN:1388-4360, eBook ISBN:978-3-030-10475-7, https://doi.org/10.1007/978-3-030-10475-7